ACS OMEGA

Open Access

http://pubs.acs.org/journal/acsodf

Article

Mechanism of the Proprietary Chinese Medicine "JiuLiWan" to Treat Ulcerative Colitis Revealed by Network Pharmacology, Molecular Docking, and Experimental Verification *In Vitro*

Zhifang Liao,[1] Xiao Liu,[1] Linxuan Li, Sikai Li, Xingxing Xing, Xiwen Zheng, Wenyu Song, Pin Gui, Qi Liu, Guanghong Rong, Yiming Shao, Mingzhi Zou,* Hongbo Liao,* and Xin Wu*

Cite This: *ACS Omega* 2025, 10, 19598−19613

Read Online

ACCESS | Metrics & More | Article Recommendations

ABSTRACT: JiuLiWan (JLW), as a classic traditional Chinese medicine formula, has been clinically used against ulcerative colitis (UC). However, the exact mechanism of its therapeutic effect remains unclear. This study aims to explore and validate the main components and pharmacological mechanism of JLW in the treatment of UC through network pharmacology, molecular docking, and cell experiments. Network pharmacology analyses indicated a total of 107 main components and 286 core targets of JLW against UC. Pathway enrichment analysis demonstrated the involvement of PI3K-AKT, MAPK, Ras, Rap1, TNF, T cell receptor, HIF-1, C-type lectin receptor, VEGF, and Th17 cell differentiation signal pathways in the efficacy of the formula. The molecular docking results indicated that the prominent components (ailanthone (AIL), butylidenephthalide, honokiol, dehydrocostuslactone, ganoderic acid A, atractylenolide I, neokurarinol, glycyrrhetinic acid, palmatine, tangeretin, and bruceine A) could bind to core targets AKT1, P53, STAT3, c-JUN, and ERK1. Subsequently, AIL was used as a representative compound to conduct cell experiments to verify its role and mechanism in anti-inflammation and immunomodulation. Interestingly, AIL could switch Jurkat T cells into a quiescence state without activating the inflammatory and immune status. However, AIL could significantly decrease the levels of interleukin-2 (IL-2) and interferon-gamma (IFN-γ), as well as the expression of surface activation markers CD69 and CD25, in PMA/ionomycin-activated Jurkat T cells by suppressing the RAF/ERK/STAT3 signaling pathway and increasing the phosphorylation of p53. This study combines network pharmacology prediction with experimental verification *in vitro* to demonstrate the mechanism of JLW in treating UC and provides an effective, safe, and inexpensive strategy for UC treatment.

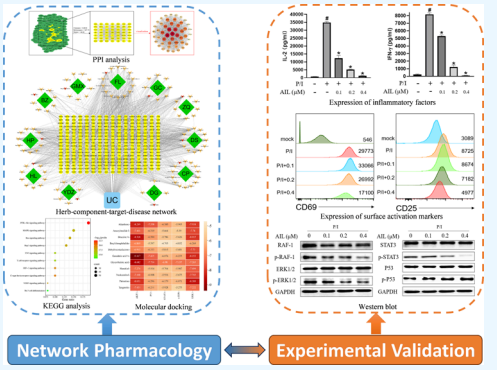

1. INTRODUCTION

Ulcerative colitis (UC) is a type of inflammatory bowel disease (IBD) that primarily affects the mucosa and submucosa of the rectum and colon. Its main symptoms include diarrhea, abdominal pain, and purulent stool.[1−3] The etiology involves environmental, genetic, and immune factors, with immune-related inflammatory responses directly linked to pathological damage to the intestinal mucosa.[4] Genome-wide association studies have identified more than 200 IBD risk alleles related to pathways involving intestinal barrier function and T cell immunity.[5−7] Drugs for UC treatment mainly include aminosalicylic acids, glucocorticoids, immunosuppressants, and biopharmaceuticals. Clinically, aminosalicylic acids and glucocorticoids are the primary treatments for mild-to-moderate UC, while moderate-to-severe UC usually uses immunosuppressants, biopharmaceuticals, or both.[8] However, these drugs have many adverse effects. For example, glucocorticoids can result in osteoporosis, depression, moon face, type 2 diabetes mellitus, and cataracts.[9] Immunosuppressants and biopharmaceuticals are usually associated with bone marrow suppression, hepatotoxicity, infections, and an increased risk of certain malignancies, such as lymphoma.[10] Moreover, the high prices of biopharmaceuticals, such as infliximab, adalimumab, golimumab, vedolizumab, and ustekinumab,[11] bring a heavy burden to the patients' families in developing countries. Therefore, there is an urgent need to seek effective, safe, and inexpensive strategies for UC treatment.

Traditional Chinese medicine (TCM), with a history of over 2000 years, has unique advantages in treating chronic diseases

Received: January 9, 2025
Revised: March 14, 2025
Accepted: March 25, 2025
Published: May 6, 2025

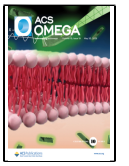

attributed to its multitarget mechanisms and few side effects. Although TCM does not have a precise equivalent for the concept of UC, its symptoms, including diarrhea and the presence of bloody mucus in stools, align with TCM categories such as diarrhea, intestinal wind, and dysentery.[12] The therapeutic purposes of TCM in treating these symptoms are to alleviate diarrhea and bleeding, reduce inflammation, and stimulate appetite.[13] TCM formulations, which consist of a combination of multiple herbs, are extensively applied in clinical treatment plans for UC. TCM prescriptions exert their effects by suppressing the release of inflammatory factors and modulating intestinal immunity to relieve the progression of UC. Classical TCM formulas, such as Huangqin Decoction,[14] Dahuang Shaoyao Decoction,[15] Lizhong Decoction,[16] and Xianglian Pills,[17] are known to regulate intestinal inflammatory mediators and cytokines, thereby enhancing the integrity of the intestinal mucosal barrier. Apart from TCM formulations, individual herbs such as *Sophora flavescens*,[18] *Salvia miltiorrhiza*,[19] *Atractylodes macrocephala*,[20] *Forsythia suspensa*,[21] and *Brucea javanica*[22] are also employed in UC treatment. Their therapeutic mechanisms are likely associated with the amelioration of immune disorders, the regulation of the inflammatory factor balance, and antioxidant properties. In recent years, with the progress of medicinal chemistry and pharmacology, there has been a surge in research on the active components of TCM. Studies have revealed that certain active constituents of TCM, including flavonoids,[23,24] polysaccharides,[25,26] and phenolic acids,[27,28] exert their therapeutic effects on UC through a range of activities, such as antimicrobial, antiviral, antioxidant, anti-inflammatory, and analgesic effects. In summary, TCM with good tolerability and accessibility has shown good efficacy in the treatment of UC in the form of prescriptions, individual herbs, or active components.

"JiuLiWan" (JLW) is a proprietary Chinese medicine approved by the China National Medical Products Administration (Approval Number: Z12020561). This formula consists of *Ailanthus altissima* (Chunpi, CP) (320g), *Angelica sinensis* (Danggui, DG) (32g), *Magnolia officinalis* (Houpo, HP) (32g), *Aucklandia lappa* (Guangmuxiang, GMX) (16g), *Poria cocos* (Fuling, FL) (16g), *Atractylodes macrocephala* (Baizhu, BZ) (16g), *Codonopsis pilosula* (Dangshen, DS) (16g), *Glycyrrhiza uralensis* (Gancao, GC) (16g), *Coptis chinensis* (Hanglian, HL) (16g), Aurantii Fructus (Zhiqiao, ZQ) (16g), and *Brucea javanica* (Yadanzi, YDZ) (2g).[29] It is well-known for its functions of strengthening the spleen and appetite, reducing inflammation, and relieving indigestion. Thus, it is used to treat dysentery, abdominal pain and bloating, constipation, lack of appetite, and fatigue. In Western medicine, these therapeutic effects correspond to the clinical manifestations of UC.[30] However, there is currently a lack of research on the mechanism of JLW in treating UC.

Network pharmacology is a strategy and technique for bioinformatics network construction and network topology analysis based on high-throughput omics data, virtual computation, and network database retrieval.[31] This approach, i.e., search of drug and disease targets by online databases, construction of drug-disease-target networks, drug disease-target correlations, identification of key compounds and targets, elucidation of the regulatory roles of drugs, and experimental validation, is extensively utilized to decipher the pharmacological mechanisms of drugs, particularly TCM with established clinical efficacy.[32] This study is the first time to reveal the effective components, potential targets, and related mechanisms of JLW in the treatment of UC based on network pharmacology and *in vitro* experimental verification.

2. MATERIALS AND METHODS

2.1. Main Compounds and Targets in JLW. The main active components of each herb in JLW were found by reviewing the Chinese Pharmacopoeia, Chinese Materia Medica, and articles in the China National Knowledge Infrastructure and Web of Knowledge. Our principles for screening compounds were as follows: (1) its bioactivity was related with inflammation and immunity; (2) its content in the corresponding herb was relatively high among all the ingredients. Then, the compound name was entered into the Pubchem database (www.pubchem.ncbi.nlm.nih.gov) to obtain the Canonical SMILES structure and imported into the SwissTargetPrediction Database (www.swisstargetprediction.ch) to obtain the corresponding targets. Moreover, the compound name was entered into the Traditional Chinese Medicine System Pharmacology Database (TCMSP, www.tcmsp-e.com) and e-pharmacophores Database (www.schrodinger.com) to obtain complementary targets. The UniProt database (www.uniprot.org) was used to correct the target protein and gene information and standardize the target nomenclature. Finally, the standardized targets were merged, and duplicates were removed.

2.2. Screening for Disease Targets in UC. The potential target genes of UC were obtained from online databases such as GeneCards (www.genecards.org), OMIM database (www.omim.org), and TTD database (www.db.idrblab.net/ttd), and duplicate genes were deleted.

2.3. Protein−Protein Interaction (PPI) Network Construction. The intersection targets of the JLW in the treatment of UC were obtained by sifting through the duplicate values of the relevant targets of the JLW and UC and then making a Venn diagram. The overlapping targets of drugs and diseases were imported into the STRING database (www.cn.string-db.org) to construct a PPI network. The species was defined as *Homo sapiens*, the minimum interaction score was limited to 0.40 to hide the unrelated nodes in the network, and the PPI network graphs of JLW for UC was obtained by Cytoscape 3.9.1 software. The targets were ranked by the Centiscape 2.2 plugin, which applied the Closeness, Betweenness, and Degree values as thresholds to select key targets by integrating multiple factors.

2.4. Herb-Component-Target-Disease Network Construction. The herbs, disease, and the above overlapping targets were imported into Cytoscape 3.9.1 software to construct the herb-component-target-disease network. The Analyze Network tool was used to calculate the Degree values for each node and filter the top-ranked components of each herb.

2.5. Gene Ontology (GO) and Kyoto Encyclopedia of Genes and Genomes (KEGG) Enrichment Analyses. The above overlapping targets were put into the Database for Annotation, Visualization and Integrated Discovery (DAVID) (www.david.ncifcrf.gov/summary.jsp) for GO and KEGG enrichment analyses in order to screen out the significant enrichment of biological process (BP), cellular component (CC), molecular function (MF), and signaling pathways. GO and KEGG analyses were visualized by the bioinformatics platform (www.bioinformatics.com.cn). A P value less than 0.05 was used as the threshold. GO analysis included BP, CC, and MF modules. According to the P value, the top 10 entries

https://doi.org/10.1021/acsomega.5c00261
ACS Omega 2025, 10, 19598−19613

were selected for each category to plot a bar graph. The top 10 enrichment results related to inflammation and immunity from KEGG analysis were displayed as a bubble chart.

2.6. Molecular Docking Study. According to the analysis of the PPI network, the core targets were selected to be used as receptors for molecular docking. The protein crystal structure used for docking was obtained from the PDB database, while the 3D structure of the compound was downloaded from the PubChem database and minimized in energy under the MMFF94 force field. This study used AutoDock Vina version 1.2.3 for molecular docking. Before the docking process was started, the receptor protein was processed with PyMol 2.5.5, which included the removal of water molecules, salt ions, and small molecules. The docking box was then set to encompass the entire protein. Furthermore, all preprocessed small molecules and the receptor protein were converted to the PDBQT format necessary for AutoDock Vina 1.2.3 using ADFRsuite 1.0.[33] During docking, the thoroughness of the global search was set to 32, with other parameters kept at default settings. The docking conformation with the highest score in the output was considered the binding conformation, and the docking results were finally visualized with PyMol 2.5.5.

2.7. Cell Culture. The Jurkat T cell line was obtained from the National Collection of Authenticated Cell Cultures (TCHU123). Jurkat T cells were cultured in RPMI 1640 medium (GIBCO, USA) supplemented with 10% fetal bovine serum (FBS, GIBCO, USA), 100 U/mL penicillin, and 100 μg/mL streptomycin (GIBCO, USA) in a 37 °C incubator with 5% CO_2 and 95% air humidity.

2.8. Cell Counting Kit-8 (CCK-8) Assay. The cell viability of Jurkat T cells was measured using a CCK-8 assay (Beyotime, China). The Jurkat T cells were seeded into 96-well plates cultured with ailanthone (AIL) (Nanjing Yuanzhi Bio, China) at 0, 0.0125, 0.025, 0.05, 0.1, 0.2, 0.4, 0.8, 1.6, and 3.2 μM for 24, 48, or 72 h. After that, the reagents for the experiments were prepared according to the instructions for use, and the CCK-8 reaction solution (Beyotime, China) was added to the appropriate sample well. Afterward, cells were cultured for another 2 h, and then, the absorbance at 450 nm of each well was measured by a microplate reader (BioTek, Agilent, Santa Clara, USA).

2.9. Cell Apoptosis Assay. Cell apoptosis was detected using an Annexin V-FITC/PI apoptosis detection kit (Beyotime, China). After culturing for 72 h with or without 0.4 μM AIL, the cells were collected, centrifuged, and resuspended in 500 μL of 1 × binding buffer. The cells were then stained in the dark at 0 °C with 5 μL of Annexin V-FITC and 5 μL of PI for 30 min. Apoptosis was measured using an Agilent NovoCyte flow cytometer (Agilent NovoCyte, Agilent, San Diego, USA), and the result was assessed using the FlowJo.

2.10. 5-Ethynyl-2′-deoxyuridine (EdU) and Hoechst Staining Assays. The EdU assay was conducted using EdU-488 Cell Proliferation Kit (Beyotime, China) according to the manufacturer's protocol. Briefly, Jurkat T cells were plated onto 6-well plates and incubated without or with AIL. The cells were divided into three groups: (1) cells cultured for 96 h without AIL; (2) cells cultured for 96 h with 0.4 μM AIL; (3) cells cultured for 72 h with 0.4 μM AIL and then cultivated for another 24 h without AIL. Subsequently, the three groups of cells were collected to incubate with 10 μM EdU each well for 2 h, fixed with 4% paraformaldehyde for 10 min, and permeabilized with 0.3% Triton X-100 for 20 min. The incorporated EdU was visualized by means of a click reaction with Fluor 488 Azide for 30 min, and the nuclear DNA was stained with Hoechst for 10 min. Finally, the proliferative cells were observed by the Agilent NovoCyte flow cytometer, and the percentage of EdU positive cells was assessed by the FlowJo.

2.11. Measurement of Extracellular Cytokines. Jurkat T cells were treated by the AIL without or with PMA (50 ng/mL) (Dibai, China)/ionomycin (1 μM) (Yuanye, China) (P/I) for 24 h. The culture supernatants were collected, and the secretion of IL-2, TNF-α, and IFN-γ was determined by enzyme-linked immunosorbent assay (ELISA) kits (Elabscience, China) according to the manufacturer's instructions.

2.12. Assessment of Surface Activation Marker Expression. The expressions of CD69 and CD25 on the Jurkat T cell surface were measured by flow cytometry. After being cultured without or with AIL and P/I for 16 h, the cells were harvested and stained with antibodies conjugated with APC or PE (BioLegend, USA) at 4 °C for 30 min. CD69 and CD25 expressions on the Jurkat T cell surface were acquired by flow cytometry and were presented in a histogram graph. Mean fluorescence intensities are shown in a bar graph.

2.13. Western Blot. Jurkat T cells stimulated in the indicated conditions or not were collected for lysis in RIPA buffer (Beyotime, China) with a phosphatase inhibitor for 30 min at 4 °C. Lysates were centrifuged at 13,500 rpm for 15 min at 4 °C, and approximately 30 μg of the lysate was separated on 8−12% SDS-PAGE gels. Proteins were transferred onto PVDF membranes (Merck Millipore, USA). Membranes were blocked in protein-free rapid blocking buffer (EpiZyme, China) for 15−30 min and incubated with the indicated primary antibodies overnight. The primary antibodies are as follows: RAS (1:1000, Signalway Antibody, China), RAF-1 (1:1000, Signalway Antibody, China), p-RAF-1 (1:1000, Signalway Antibody, China), MEK1/2 (1:1000, Signalway Antibody, China), p-MEK1/2 (1:1000, Signalway Antibody, China), ERK1/2 (1:2000, Proteintech, China), p-ERK1/2 (1:2000, Proteintech, China), STAT3 (1:750, Signalway Antibody, China), p-STAT3 (1:750, Signalway Antibody, China), PI3K (1:5000, Proteintech, China), AKT (1:750, Signalway Antibody, China), p-AKT (1:2000, Proteintech, China), mTOR (1:1000, Signalway Antibody, China), NF-κB (1:750, Signalway Antibody, China), p-NF-κB (1:750, Signalway Antibody, China), c-JUN (1:1000, Signalway Antibody, China), P53 (1:1000, Signalway Antibody, China), p-P53 (ser15) (1:750, Signalway Antibody, China), and GAPDH (1:5000, Signalway Antibody, China). Excess primary antibodies were discarded by washing the membrane three times with TBST, and then, the membrane was incubated with 0.1 μg/mL peroxidase-labeled secondary antibodies (rabbit antimouse or goat antirabbit IgG, 1:20000, Signalway Antibody, China) for 1 h. After washing with TBST three times, bands were visualized with ECL Western blotting detection reagents (Beyotime, China) on an Azure 600 (Azure Biosystems, Dublin, USA).

2.14. Statistical Analysis. GraphPad Prism 8.0 software was used for the analysis. Experiment data are presented as mean ± SD and were analyzed using the unpaired Student's t test and one-way analysis of variance. All experiments were carried out in dependent triplicates. Hypergeometric tests were used to calculate the p value for GO and KEGG enrichment analysis. Usually, a p value less than 0.05 was set as the threshold and considered to indicate statistical significance.

https://doi.org/10.1021/acsomega.5c00261
ACS Omega 2025, 10, 19598−19613

Table 1. Main Components in the Herbs of JLW

herbs	components	amount
Ailanthus altissima (Chunpi, CP)	1-hydroxycanthin-6-one, 1-methoxycanthin-6-one, 5-hydroxy-4-methoxycanthin-6-one, ailanthone, ailantinol A, amarolide, amarolide-11-acetate, canthin-6-one, neoquassine, quassin, shinjudilactone, shinjulactone A, shinjulactone B, shinjulactone K	14
Angelica sinensis (Danggui, DG)	butylidenephthalide, ferulic acid, *Z*-6,8′,7,3′-diligustilide, *Z*-ligustilide	4
Magnolia officinalis (Houpo, HP)	honokiol, isomagnolol, magnaldehyde B, magnaldehyde D, magnatriol B, magnolol, magnolignan A, magnolignan C, tetrahydromagnolol, α-eudesmol, β-eudesmol	11
Aucklandia lappa (Guangmuxiang, GMX)	alantolactone, costuslactone, dehydrocostuslactone, dihydrocostunolide, α-costol, α-cyclocostunolide, β-costol, β-cyclocostunolide, γ-costol	9
Poria cocos (Fuling, FL)	pachymic acid, tumulosic acid, 3-*O*-acetyl-16α-hydroxytrametenolic acid, 16α-hydroxytrametenolic acid, ganoderic acid A, dehydrotrametenolic acid, dehydropachymic acid, 3-epidehydropachymic acid, 29-hydroxydehydrotumulosic acid, dehydroburicoic acid monoacetate, poricoic acid G, poricoic acid H, daedaleanic acid A, β-amyrin acetate, 3-acetyl oleanolic acid	15
Atractylodes macrocephala (Baizhu, BZ)	aromadendrene, atractylenolide II, atractylenolide IV, atractylon, atractyloside A, β-elemene, biatractylolide, atractylenolide I	8
Codonopsis pilosula (Dangshen, DS)	apigenin, chrysoeriol, codonopsine, codotubulosine A, hesperidin, kaempferol, lobetyolin, luteolin, neokurarinol, nicotine, quercetin, tricin, wogonin	13
Glycyrrhiza uralensis (Gancao, GC)	glabrolide, glycyrrhetinic acid, glycyrrhizic acid, isoliquiritin, isoliquiritingenin, licochalcone, liquiritigenin, liquiritin	8
Coptis chinensis (Hanglian, HL)	berberastine, berberine, columbamine, coptisine, epiberberine, jatrorrhizine, magnoflorine, palmatine, tetrandrine, worenine	10
Aurantii Fructus (Zhiqiao, ZQ)	2-undecanone, hesperidin, limonene, naringin, nobiletin, tangeretin, α-terpineol, β-caryophyllene, β-myrcene	9
Brucea javanica (Yadanzi, YDZ)	bruceanic acid E, bruceanic acid F, bruceantin, bruceine A, bruceantinol B, bruceanic acid E methyl ester, dihydrobruceantin	7

3. RESULTS

3.1. Main Components in JLW and Their Targets. As can be seen in Table 1, 107 main components were identified by reviewing the information on JLW's herbs in Chinese Pharmacopoeia, Chinese Materia Medica, and articles about ingredient extraction and separation. Target prediction was performed through the TCMSP, PubChem database, SwissTargetPrediction database, and e-pharmacophores database. Also, the UniProt database was used to normalize the target names and exclude their duplicates to result in a total of 837 targets.

3.2. Disease Targets in UC. The keyword "Ulcerative Colitis" was entered into the GeneCards, OMIM, and TTD databases with the search scope of "Homo sapiens" to obtain human UC genes. The top 2000 disease targets in the GeneCards database were retained according to their relevance score, while all the genes in OMIM and TTD databases were reserved. Finally, 2030 disease targets related to UC were obtained after deletion of duplicate genes from those three databases.

3.3. PPI Network Analysis. The "JLW-UC" target Venn diagram (Figure 1A) was constructed by intersecting herb targets with disease targets, and a total of 286 intersection targets were obtained. The 286 targets were uploaded to the STRING database for PPI network construction. Then, Cytoscape 3.9.1 software was used to automatically analyze the Closeness, Betweenness, and Degree values, which obtained the following results: Closeness = 0.001839822, Betweenness = 267.7333333, and Degree = 46.05614035. These three values were employed as thresholds for screening core targets. The PPI analysis remained 49 nodes and 933 edges after filtering, as shown in Figure 1B. According to the Degree value, AKT1, P53, STAT3, JUN (c-JUN), and MAPK3 (ERK1) were identified as core targets.

3.4. Herb-Component-Target-Disease Network Analysis. Cytoscape 3.9.1 software was utilized to construct the herb-component-target-disease network (Figure 1C), in which a higher Degree value of a node indicates a greater level of connectivity with other nodes. Taking into account the synergistic relationships in the compatibility of each herb, the Degree values of compounds ranking at the top for each herb were selected as the prominent components, which included ailanthone (CP), butylidenephthalide (DG), honokiol (HP), dehydrocostuslactone (GMX), ganoderic acid A (FL), atractylenolide I (BZ), neokurarinol (DS), glycyrrhetinic acid (GC), palmatine (HL), tangeretin (ZQ), and bruceine A (YDZ).

3.5. Enrichment Analysis of GO and KEGG. GO and KEGG enrichment analyses were performed on the 286 intersection targets, which used the DAVID database to uncover the mechanisms of JLW in UC treatment. GO enrichment analysis (Figure 2A) showed that the targets involved 1136 significant items ($p < 0.05$), in which 858 items were related to BP, mainly involving inflammatory response, protein phosphorylation, and regulation of the ERK1/2 cascade. 98 items were related to CC, mainly involving plasma membrane, cytoplasm, and cytosol. A total of 180 items were associated with MF, mainly involving protein binding, ATP binding, and enzyme binding. A total of 172 KEGG enriched pathways ($p < 0.05$) (Figure 2B) were identified, in which the top 10 pathways associated with inflammation and immunity were PI3K-AKT, MAPK, Ras, Rap1, TNF, T cell receptor, HIF-1, C-type lectin receptor, VEGF, and Th17 cell differentiation signal pathways.

3.6. Molecular Docking between Prominent Components and Core Targets. According to the analysis of PPI and the herb-component-target-disease network, molecular docking was applied to further research the drug−receptor interactions between prominent components and core targets. The optimal binding energy of proteins and components in molecular docking is shown in Figure 3. A darker color in the diagram means lower binding energy, which corresponds to a higher likelihood of ligand−receptor binding and better affinity. The top five compounds with the lowest binding

https://doi.org/10.1021/acsomega.5c00261
ACS Omega 2025, 10, 19598−19613

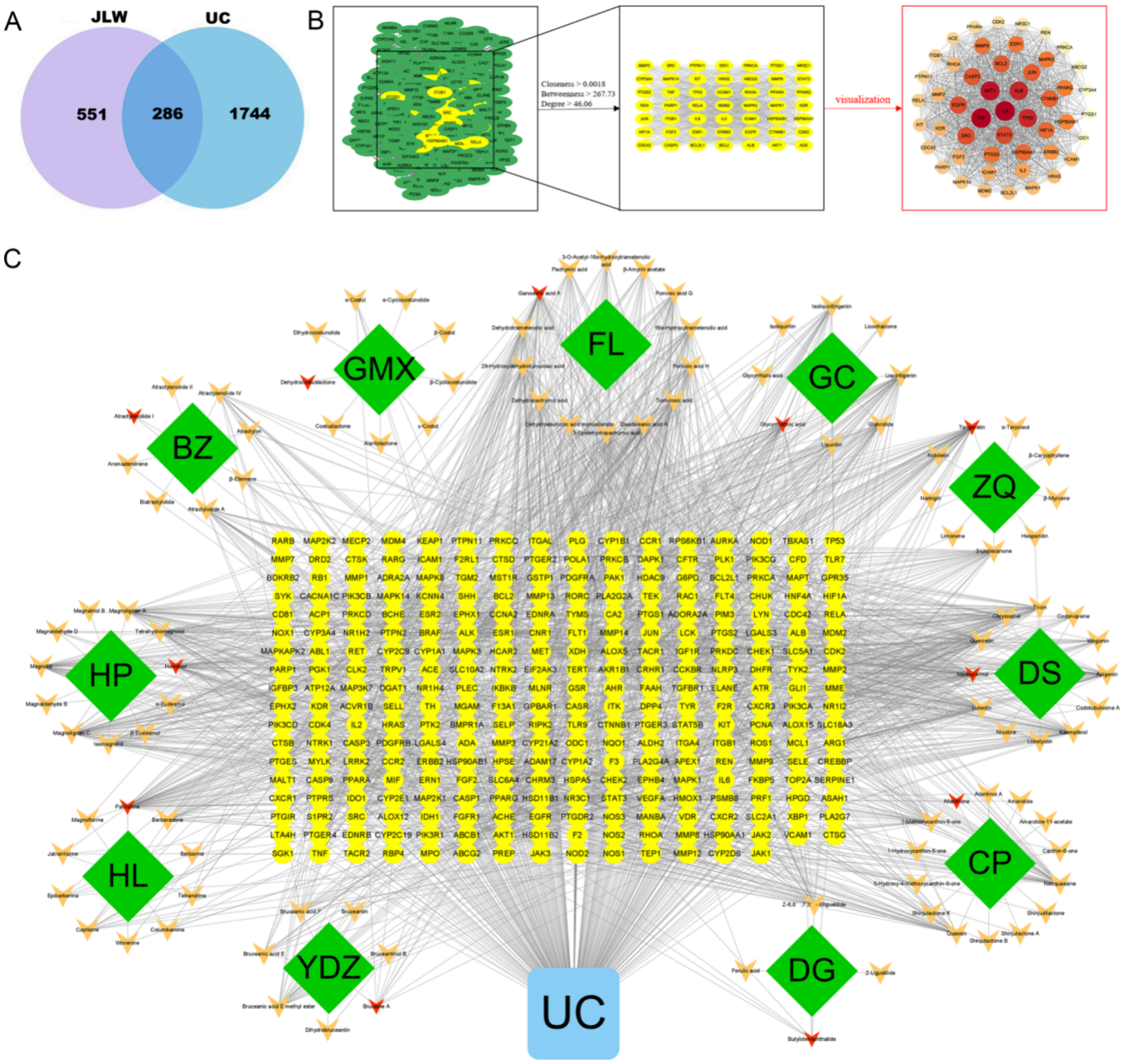

Figure 1. Results of network pharmacology analyses of JLW against UC. (A) Venn diagram of the targets of UC and JLW. (B) The result of PPI analysis for intersection targets. A deeper-colored, larger circle indicates a greater degree value and a more important target. (C) Herb-component-target-disease network. The green diamonds represent the herbs of JLW, the orange nodes represent the components, the red nodes represent the prominent components of each herb, the yellow ellipses represent the targets, and the blue round rectangles represent the disease. The edge represents the interactions between herb-component, component-target, and target-disease.

energies to the five core targets were selected and docked. The 3D ligand interactions are shown in Figure 4, in which the left image is a global view, the right image is a partial view, the yellow stick is a small molecule, the cyan cartoon is a protein, the blue line represents hydrogen bonding whose formation makes the kinase bind more tightly to the small molecules, and the gray dotted line represents hydrophobic whose interactions are the basis for the binding of the small molecule to the protein. Ailanthone interacted with AKT1 protein in GLY-294, LEU-295, and LYS-276 by forming hydrogen bonds in PHE-161 hydrophobically (Figure 4a). Bruceine A interacted with AKT1 protein in LYS-276, LEU-295, and GLU-191 by forming hydrogen bonds in ASP-292, LEU-159, and VAL-164 hydrophobically (Figure 4b). Ganoderic acid A interacted with AKT1 protein in ASP-292, THR-160, GLU-234, and ASN-279 by forming hydrogen bonds in PHE-161, VAL-164, THR-211, LEU-156, and THR-291 hydrophobically (Figure 4c). Glycyrrhetinic acid interacted with AKT1 protein in ASP-439, PHE-161, and GLY-162 by forming hydrogen bonds in LYS-179, GLU-278, VAL-164, PHE-442, and PHE-236 hydrophobically (Figure 4d). Palmatine interacted with AKT1 protein in ALA-230 by forming a hydrogen bond in LYS-179, VAL-164, and LEU-156 hydrophobically (Figure 4e). Ailanthone interacted with c-JUN protein in ARG-276, ARG-279, and ARG-272 by forming a hydrogen bond (Figure 4f). Ganoderic acid A interacted with c-JUN protein in GLU-

https://doi.org/10.1021/acsomega.5c00261
ACS Omega 2025, 10, 19598−19613

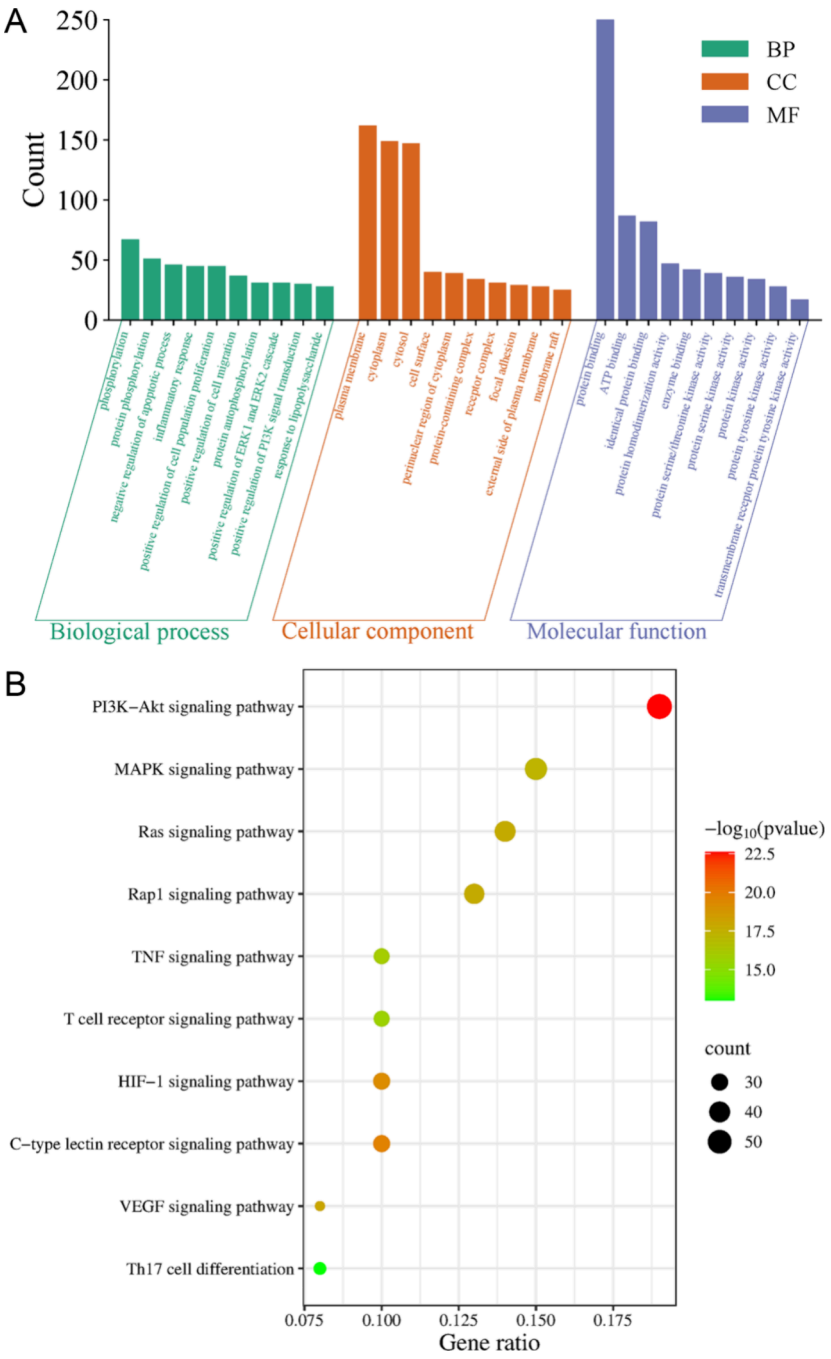

Figure 2. GO and KEGG analysis. (A) The top 10 BP, MF, and CC from the GO analysis. (B) The top 10 inflammation and immune related pathways from the KEGG analysis.

275, ARG-276, and ARG-279 by forming hydrogen bonds in LEU-280 and ARG-272 hydrophobically (Figure 4g). Glycyrrhetinic acid interacted with c-JUN protein in ARG-276, LYS-283, LYS-285, GLU-281, and LEU-280 by forming the van der Waals energy (Figure 4h). Honokiol interacted with c-JUN protein in GLU-275 and ARG-272 by forming hydrogen bonds in ARG-276, GLU-275, ARG-279, ARG-272, LYS-273, and LEU-280 hydrophobically (Figure 4i). Palmatine interacted with c-JUN protein in GLU-275 by forming hydrogen bonds in LEU-280, GLU-275, ARG-276, and ARG-279 hydrophobically (Figure 4j). Ailanthone interacted with ERK1 protein in LYS-168, ASP-128, and SER-170 by forming hydrogen bonds in VAL-56 and LEU-173 hydrophobically (Figure 4k). Atractylenolide I interacted with ERK1 protein in ALA-69, LEU-173, ILE-101, VAL-56, ILE-48, and GLN-122 by forming the van der Waals energy (Figure 4l). Bruceine A interacted with ERK1 protein in VAL-56, ASP-184, and SER-170 by forming a hydrogen bond in TYR-53, ILE-73, and VAL-56 hydrophobically (Figure 4m). Ganoderic acid A interacted with ERK1 protein in ASP-128 and MET-125 by forming a hydrogen bond in ILE-48 and MET-125 hydrophobically (Figure 4n). Palmatine interacted with ERK1 protein in THR-127 and ASP-128 by forming hydrogen bonds in ALA-69, ILE-48, and LEU-173 hydrophobically (Figure 4o). Ailanthone interacted with p53 protein in GLU-180 by forming a hydrogen bond in PRO-177 hydrophobically (Figure 4p). Bruceine A interacted with

https://doi.org/10.1021/acsomega.5c00261
ACS Omega 2025, 10, 19598−19613

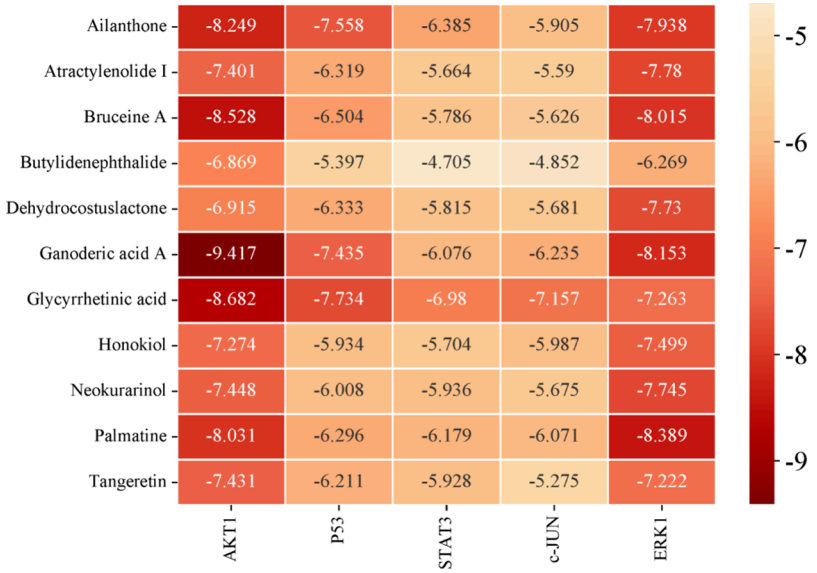

Figure 3. Optimal binding energy of core targets and prominent components in molecular docking.

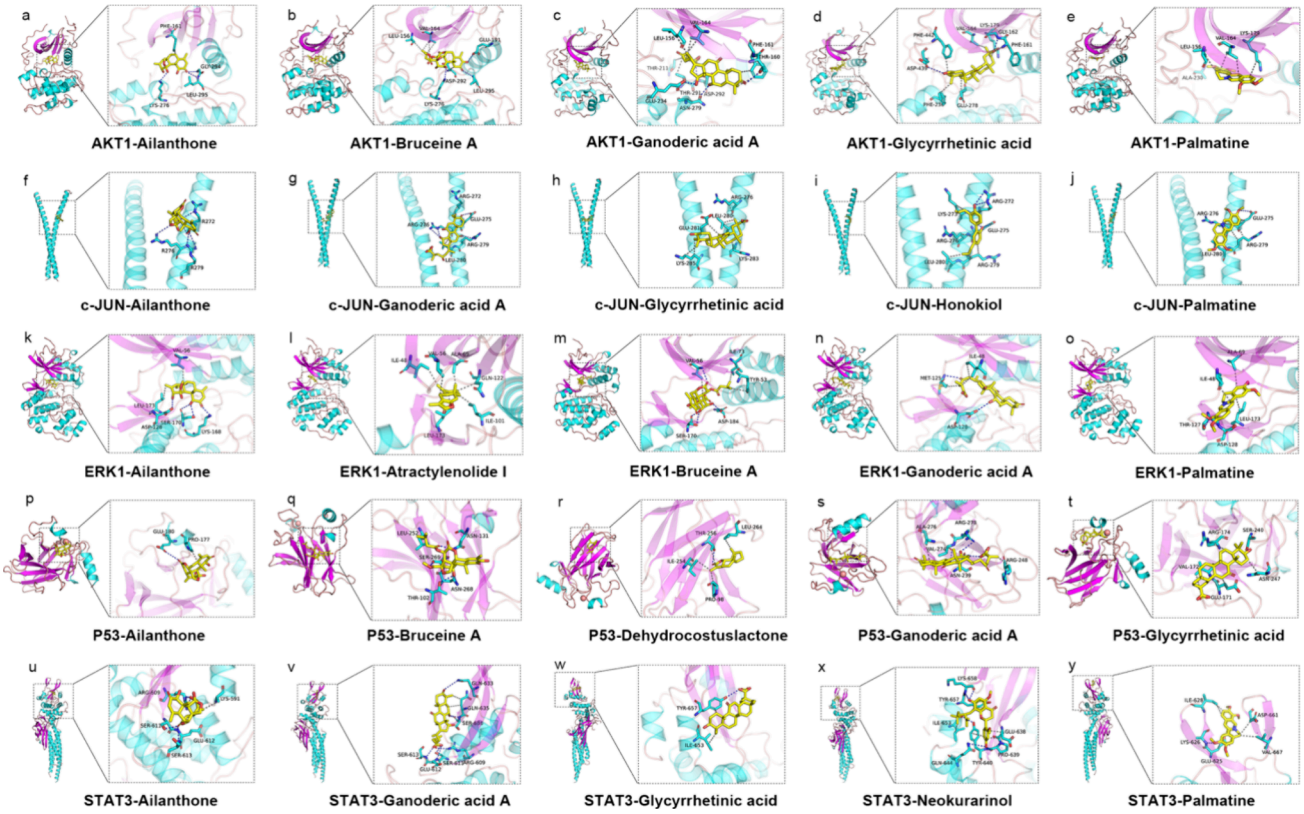

Figure 4. Representative docking complex of components and targets. (a) Ailanthone with AKT1. (b) Bruceine A with AKT1. (c) Ganoderic acid A with AKT1. (d) Glycyrrhetinic acid with AKT1. (e) Palmatine with AKT1. (f) Ailanthone with c-JUN. (g) Ganoderic acid A with c-JUN. (h) Glycyrrhetinic acid with c-JUN. (i) f Honokiol with c-JUN. (j) Palmatine with c-JUN. (k) Ailanthone with ERK1. (l) Atractylenolide I with ERK1. (m) Bruceine A with ERK1. (n) Ganoderic acid A with ERK1. (o) Palmatine with ERK1. (p) Ailanthone with p53. (q) Bruceine A with p53. (r) Dehydrocostuslactone with p53. (s) Ganoderic acid A with p53. (t) Glycyrrhetinic acid with p53. (u) Ailanthone with STAT3. (v) Ganoderic acid A with STAT3. (w) Glycyrrhetinic acid with STAT3. (x) Neokurarinol with STAT3. (y) Palmatine with STAT3.

p53 protein in THR-102, SER-269, ASN-131, and ASN-268 by forming a hydrogen bond in LEU-252 hydrophobically (Figure 4q). Dehydrocostuslactone interacted with p53 protein in THR-256 by forming a hydrogen bond in ILE-254, LEU-264, PRO-98, and THR-256 hydrophobically (Figure 4r). Ganoderic acid A interacted with p53 protein in ASN-239, VAL-274, and ARG-273 by forming a hydrogen bond in ALA-276 and ARG-248 hydrophobically (Figure 4s). Glycyrrhetinic acid interacted with p53 protein in SER-240 by forming hydrogen bonds in GLU-171, ARG-174, ASN-247, and VAL-172 hydrophobically (Figure 4t). Ailanthone interacted with STAT3 protein in ARG-609, GLU-612, SER-613, and SER-

https://doi.org/10.1021/acsomega.5c00261
ACS Omega 2025, 10, 19598−19613

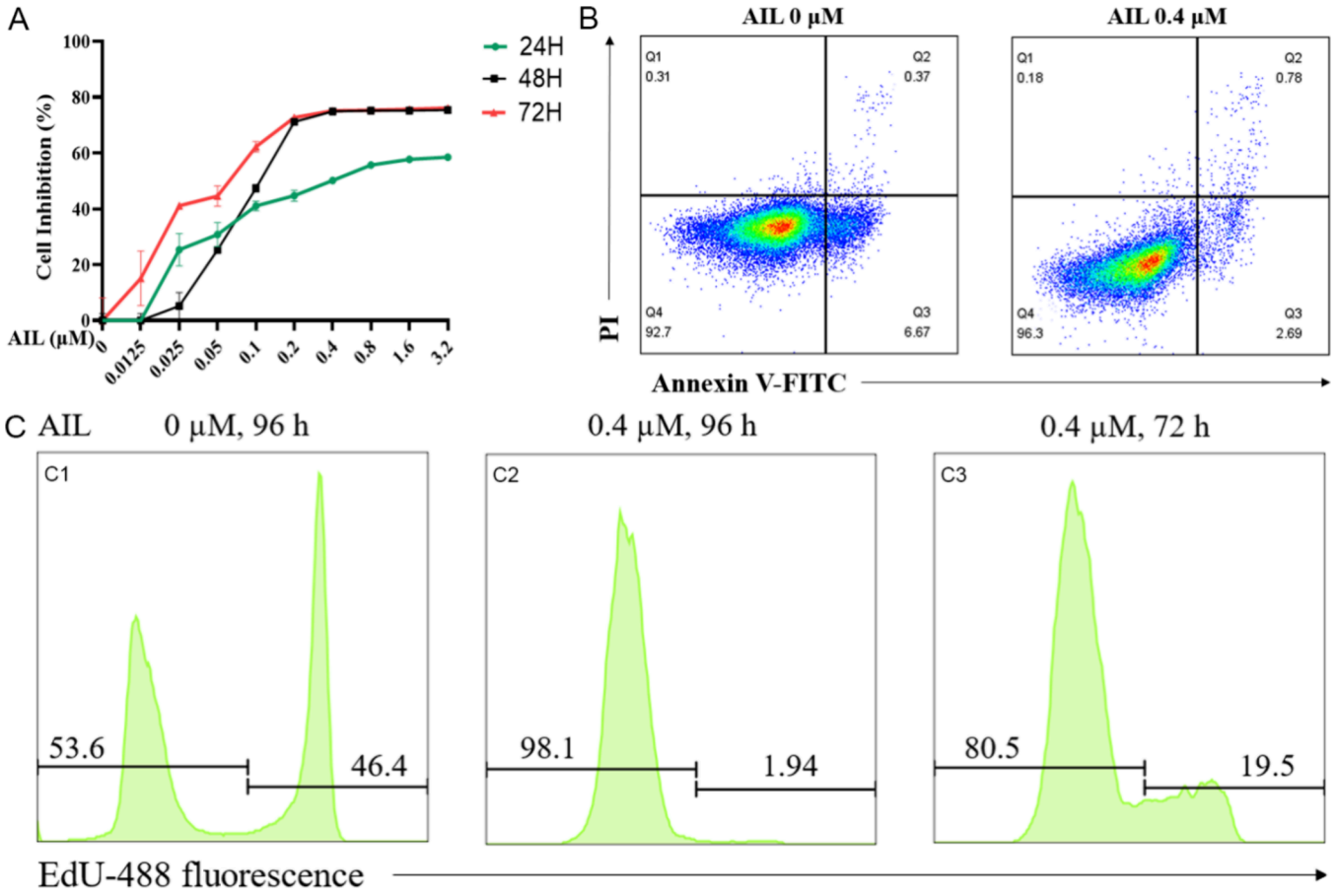

Figure 5. AIL inhibits cell growth without cytotoxicity. (A) The proliferation inhibition ability of AIL on Jurkat T cells tested by the CCK-8 assay. (B) Annexin V-FITC/PI dual staining of Jurkat T cells treated with AIL at 0 or 0.4 μM AIL for 72 h detected by flow cytometry. (C) The percentages of EdU positive cells were detected by flow cytometry after being cultured without or with AIL. Cells were cultured for 96 h without AIL (C1); cells were treated with 0.4 μM AIL for 96 h (C2); cells were treated with 0.4 μM AIL for 72 h and then cultured for another 24 h without AIL (C3).

611 by forming hydrogen bonds in LYS-591 hydrophobically (Figure 4u). Ganoderic acid A interacted with STAT3 protein in SER-613, GLU-612, SER-611, GLN-633, SER-636, and ARG-609 by forming hydrogen bonds in GLN-635 hydrophobically (Figure 4v). Glycyrrhetinic acid interacted with STAT3 protein in TYR-657 by forming hydrogen bonds in ILE-653 and TYR-657 hydrophobically (Figure 4w). Neokurarinol interacted with STAT3 protein in LYS-658, TYR-640, GLN-644, and PRO-639 by forming hydrogen bonds in GLU-638, TYR-640, ILE-653, and TYR-657 hydrophobically (Figure 4x). Palmatine interacted with STAT3 protein in LYS-626 by forming a hydrogen bond in GLU-625, VAL-667, ILE-628, and ASP-661 hydrophobically (Figure 4y).

3.7. AIL Inhibits Jurkat T Cell Growth without Cytotoxicity. *Ailanthus altissima* (Chunpi, CP), constituted the highest weight ratio (64%) of the formula JLW, is rich in quassinoids that may have a certain therapeutic effect on UC based on their excellent antitumor, antiviral, anti-inflammation, and antibacterial activities.[34−36] Its main quassinoid, AIL, was regarded as one of the prominent components in the above network pharmacology study, which showed that AIL might target AKT1, p53, STAT3, c-JUN and ERK1 to regulate inflammation and immune related pathways, such as PI3K/AKT, MAPK, Ras, T cell receptor, TNF, and Th-17 signaling pathways. Furthermore, AIL was reported to have a lot of activities such as anticancer, anti-inflammatory, antibacterial, and herbicidal effects.[36] Thus, AIL was used as a representative compound to conduct *in vitro* experiments on Jurkat T cells to verify its role and mechanism in anti-inflammation and immunomodulation. Interestingly, although AIL dramatically inhibited Jurkat T cells growth with IC_{50} values of 0.57 ± 0.17, 0.15 ± 0.05, and 0.07 ± 0.02 μM at 24, 48, and 72 h, respectively (Figure 5A), it did not show cytotoxicity even at a concentration of 0.4 μM up to 72 h, which was supported by the flow cytometry assay results (Figure 5B). Amazingly, the Jurkat T cells reproliferated gradually after AIL was withdrawn (Figure 5C) detected by EdU staining assays. The percentage of EdU positive cells at 46.4% displayed their proliferative ability after culturing for 96 h without AIL (Figure 5C1), while the percentage at 1.94% implied that almost their growth capacity totally lost after culturing for 96 h with 0.4 μM AIL (Figure 5C2). Moreover, the cells returned to proliferate partly with 19.5% of EdU positive cells after 72 h of treatment with 0.4 μM AIL and another 24 h without AIL (Figure 5C3). In other words, AIL could switch Jurkat T cells into a quiescence state.

3.8. AIL Suppresses Inflammatory Cytokines in Activated Jurkat T Cells. IL-2, TNF-α, and IFN-γ secreted by Jurkat T cells play an important role in immune responses. Thus, the effects of AIL on these inflammatory factors were tested and the results displayed that AIL had no significant effect on them in unactivated Jurkat T cells (Figure 6A−C).

https://doi.org/10.1021/acsomega.5c00261
ACS Omega 2025, 10, 19598−19613

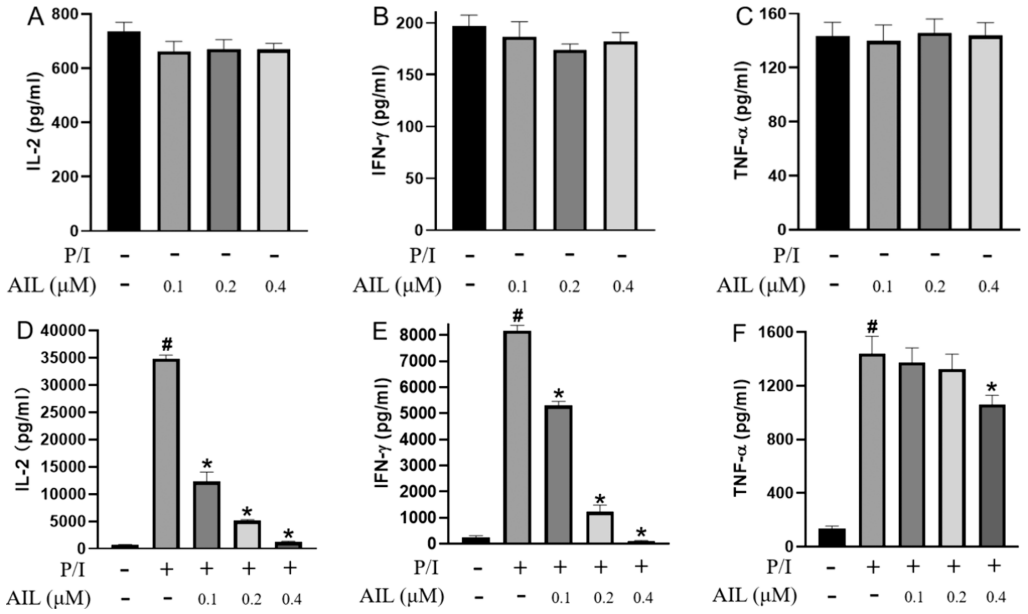

Figure 6. Secretion of inflammatory cytokines in Jurkat T cells treated by AIL with or without P/I. (A−C) IL-2, TNF-α, and IFN-γ from supernatants of Jurkat T cells with AIL treatment alone for 24 h. (D−F) IL-2, TNF-α, and IFN-γ from supernatants of Jurkat T cells with AIL and P/I treatment for 24 h. The mean value ± SEM is presented in the bar graph. $^{\#}P < 0.05$ vs control group, $^{*}P < 0.05$ vs model group.

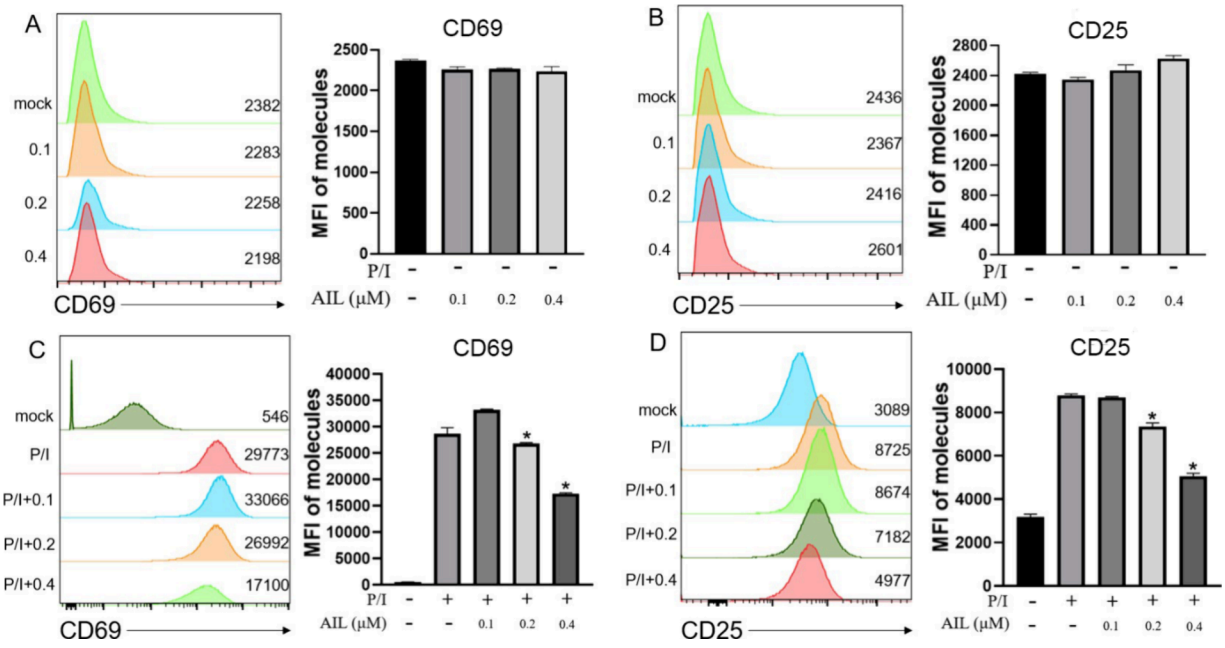

Figure 7. Expression of surface molecules in Jurkat T cells treated by AIL with or without P/I. (A, B) Jurkat T cells were treated with AIL for 16 h without P/I. (C, D) Jurkat T cells were treated with AIL for 16 h with P/I. The mean value ± SEM of CD69 and CD25 is presented in the bar graph. $^{\#}P < 0.05$ vs control group, $^{*}P < 0.05$ vs model group.

Interestingly, when Jurkat T cells were stimulated with P/I, the levels of IL-2 (Figure 6D) and IFN-γ (Figure 6E) were significantly suppressed by AIL dose-dependently, especially at a concentration of 0.4 μM. However, TNF-α (Figure 6F) could not be inhibited if taking the cell amount into consideration. That is to say, AIL selectively inhibited the secretion of IL-2 and IFN-γ in activated Jurkat T cells, but not TNF-α, and had no impact on the inflammatory cytokine secretion function in unactivated Jurkat T cells.

3.9. AIL Reduces the Expression of Surface Activation Markers in Activated Jurkat T Cells. It has been reported that the surface activation markers of T cells, such as CD69 and CD25, exhibit their immune status and will increase when they are activated.[37] CD69 and CD25 not only play key roles in immune activation, regulation, and cell signaling but also are involved in the functional regulation of T cells, which is crucial for maintaining immune balance and responding to immune response.[38] Thus, the expressions of CD69 and CD25 in unactivated and activated T cells were assessed by flow cytometry. AIL did not affect the expression of CD69 (Figure 7A) or CD25 (Figure 7B) in unactivated Jurkat T cells. However, CD69 (Figure 7C) and CD25 (Figure 7D) were

https://doi.org/10.1021/acsomega.5c00261
ACS Omega 2025, 10, 19598−19613

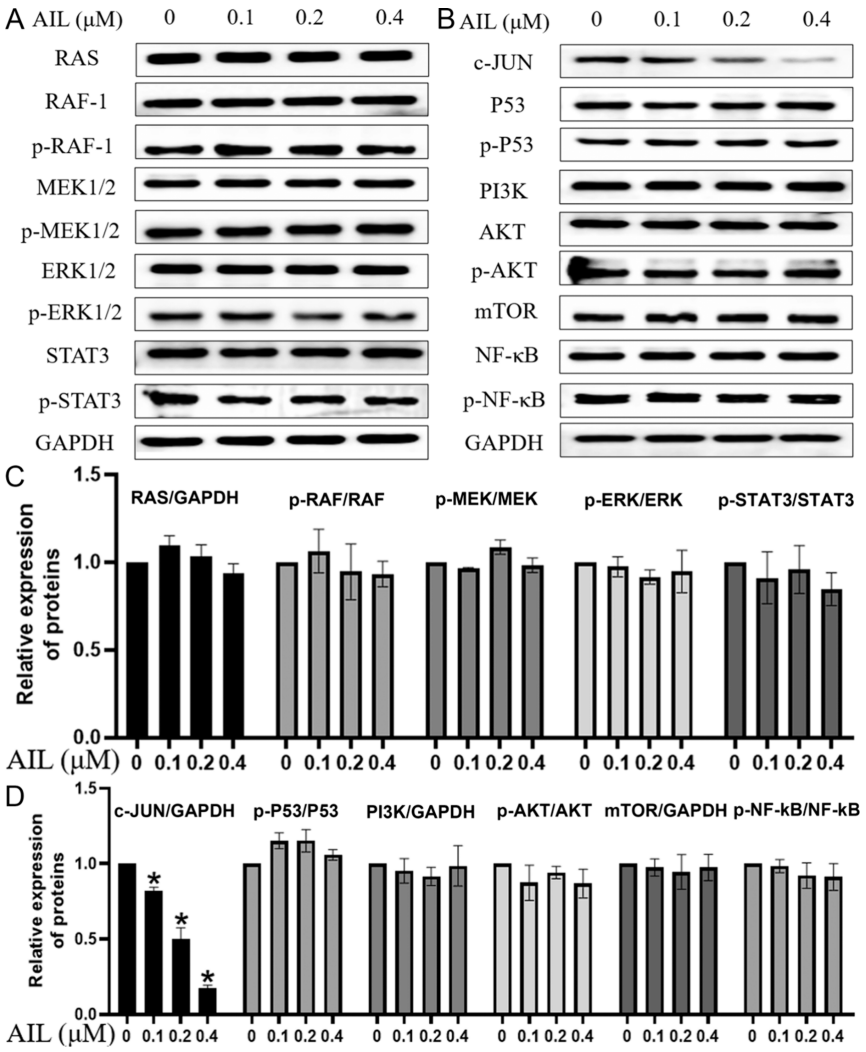

Figure 8. Analysis on related proteins in Jurkat T cells treated by AIL without P/I for 24 h. (A, B) Western blot on proteins of unactivated Jurkat T cells. (C, D) Densitometric values were normalized to those of the control group. Results are presented as mean ± standard deviation ($n = 3$), *$P <$ 0.05 vs control group.

suppressed by treatment with AIL in activated Jurkat T cells, especially at concentrations of 0.2 and 0.4 μM.

3.10. AIL Suppressed the RAF/ERK/STAT3 Pathway in Activated Jurkat T Cells. The network pharmacology study showed that AIL might target AKT1, P53, STAT3, c-JUN, and ERK1 to regulate PI3K/AKT, MAPK, and Ras signaling pathways. But the results exhibited that AIL had no influence on most proteins related with these pathways except for c-JUN in unactivated Jurkat T cells as shown in Figure 8. Interestingly, in activated Jurkat T cells, AIL could reduce the level of RAF-1, decrease the phosphorylation of RAF-1, ERK1/2, and STAT3, increase the phosphorylation of p53, and diminish the level of c-JUN while not impacting the contents of RAS, MEK, p-MEK, and the proteins related with the PI3K/AKT signaling pathway, i.e., PI3K, AKT, mTOR, and NF-κB (Figure 9). These results suggested that AIL could not interfere with unactivated Jurkat T cells but could exert its inhibitory effect on the inflammatory response against activated Jurkat T cells by suppressing the RAF/ERK/STAT3 signaling pathway and increasing p-p53. Furthermore, these proteins in the MAPK signaling pathway, i.e., RAF-1, p-RAF-1, p-ERK1/2, STAT3, p-STAT3, were found to be upregulated when Jurkat T cells were stimulated with P/I (Figure 10). This could be responsible for the sharp increase in the levels of IL-2 (Figure 6D) and IFN-γ (Figure 6E) in activated Jurkat T cells. When T cells are under stress, the level of p-p53 could be rapidly increased and activated to exhibit its anti-inflammatory activity in a positive feedback manner.[39,40] Thus, the increase of p-p53 (Figure 10) in P/I-treated Jurkat T cells should be induced by the stimulation of inflammatory cytokine surge, which was prompted by the activation of the RAF/ERK/STAT3 signaling pathway. Meanwhile, the level of p-P53 increased further in P/I-treated Jurkat T cells (Figure 9), which showed the enhancement of its anti-inflammatory effect by AIL. The above results suggested that AIL is an effective anti-inflammatory and immunosuppressive agent without interfering with normal Jurkat T cells.

4. DISCUSSION

In recent years, the rising incidence of UC has become a significant concern in the medical community. This chronic intestinal disorder has an exceedingly intricate pathogenesis, with its underlying causes still not fully understood.[41] Nonetheless, a multitude of studies highlight the pivotal role of aberrant inflammatory and immune reactions in the progression of UC, which are broadly acknowledged as key

https://doi.org/10.1021/acsomega.5c00261
ACS Omega 2025, 10, 19598−19613

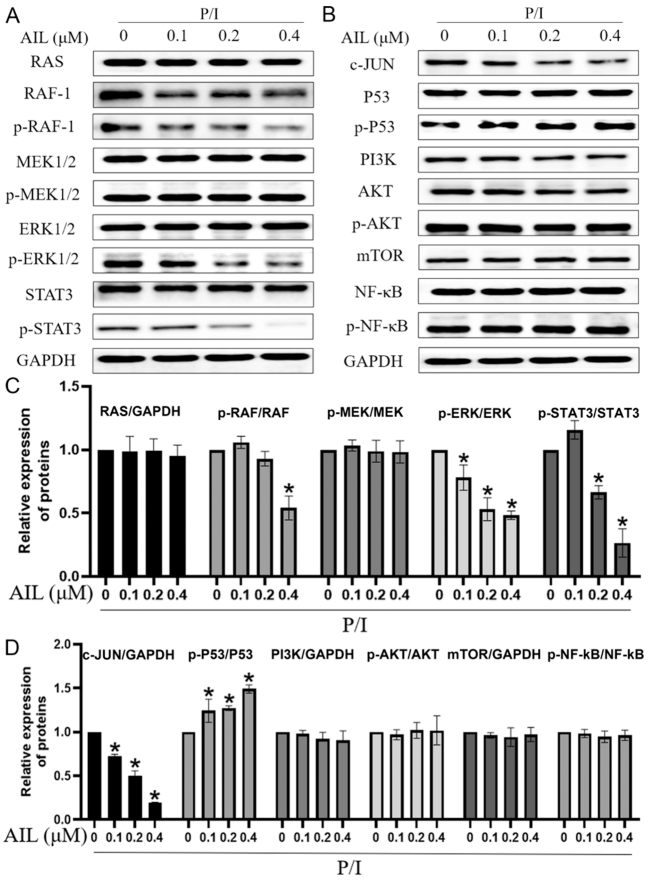

Figure 9. Analysis on related proteins in Jurkat T cells treated by AIL with P/I for 24 h. (A, B) Western blot on proteins of activated Jurkat T cells treated by AIL for 24 h. (C, D) Densitometric values were normalized to those of the control group. Results are presented as mean ± standard deviation (n = 3), *P < 0.05 vs control group.

internal factors contributing to intestinal inflammation and tissue damage in affected individuals.[42,43] To alleviate patients' suffering, researchers are diligently pursuing effective therapeutic strategies, with a particular emphasis on modulating the inflammatory immune responses and improving prognosis. Among various treatment approaches, TCM distinguishes itself as a notable option due to its holistic perspective, multi-components, and multitargets, which have been confirmed to be effective in mitigating UC symptoms.[44−46]

JLW is an ancient TCM prescription and is approved as a proprietary Chinese medicine for the treatment of UC, but its specific mechanisms still need to be explored. Network pharmacology and molecular docking techniques are auxiliary means to explore the mechanisms of drugs, which can be used to comprehensively predict and analyze the active components of TCM and identify potential targets and signaling pathways.[32,47] This study investigated the main active components and possible mechanisms of JLW in the treatment of UC by network pharmacology and molecular docking. Through extensive analysis on literature, 107 main components were obtained for the JLW treatment in UC, and through network topology analysis, the prominent components of each herb were ultimately identified as ailanthone, butylidenephthalide, honokiol, dehydrocostuslactone, ganoderic acid A, atractylenolide I, neokurarinol, glycyrrhetinic acid, palmatine, tangeretin, and bruceine A. All these components were found to have anti-inflammatory and immune-modulating effects.[48−58]

The PPI and KEGG analyses of intersection targets suggested that JLW might treat UC through core targets such as AKT1, P53, STAT3, JUN (c-JUN), and MAPK3 (ERK1), which were significantly enriched in PI3K/AKT, MAPK, Ras, and T cell receptor signaling pathways. The molecular docking confirmed that the 11 prominent components have good binding ability to AKT1, P53, STAT3, JUN (c-JUN), and MAPK3 (ERK1). This article mainly investigated the regulatory effects of AIL on inflammation and immune responses in both activated and unactivated Jurkat T cells. When Jurkat T cells were activated with P/I, they produced substantial amounts of IL-2, which was regarded as a valuable model for studying T cell-related inflammation and immunity.[59] AIL suppressed the secretion of inflammatory cytokines IL-2 and IFN-γ and the expression of surface activation markers CD69 and CD25. Western blot analyses demonstrated that AIL reduced the level of phosphorylation of proteins in the RAF/ERK/STAT3 signaling pathway and upregulated the level of phosphorylation of p53. However, these changes were not observed in the unactivated Jurkat T cells. Moreover, AIL had no influence on the proteins in the PI3K/AKT/mTOR pathway or NF-κB whether in activated or unactivated Jurkat T cells. These findings suggest that AIL may mitigate excessive immune

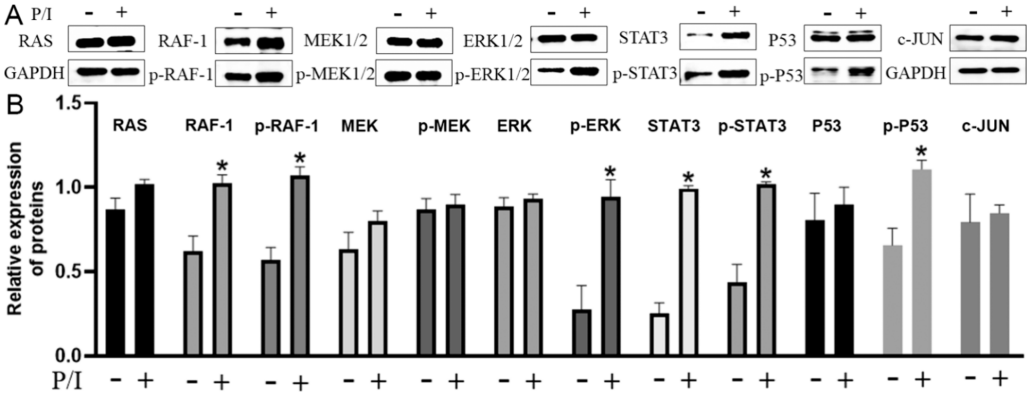

Figure 10. Analysis on related proteins in Jurkat T cells cultured with or without P/I for 24 h. (A) Western blot on proteins of Jurkat T cells. (B) Densitometric values were normalized to those of the control group. Results are presented as mean ± standard deviation (n = 3), *P < 0.05 vs control group.

https://doi.org/10.1021/acsomega.5c00261
ACS Omega 2025, 10, 19598−19613

responses by suppressing the RAF/ERK/STAT3 pathway and enhancing p-p53 protein levels, which offers a potential therapeutic approach for the treatment of UC.

PMA and ionomycin can activate the T cells by the TCR signaling pathway characterized by the increase of CD69 and CD25.[60−63] The activated T cells begin to proliferate massively and secrete a large amount of inflammatory factors, which further recruit and activate immune cells to cause tissue inflammation and damage.[64,65] In this study, we confirmed that the expression of CD69 and CD25 was significantly decreased after treatment with AIL in activated Jurkat T cells. This suggests that AIL suppresses the immune response through the TCR signaling pathway. After the TCR signaling pathway is activated, it can function through a series of downstream signaling pathways, such as MAPK, PI3K-AKT-mTOR, NF-κB, and other signaling pathways. The MAPK signaling pathway can be activated by extracellular stimuli, and then, the Ras protein is activated to recruit and activate Raf kinase. Subsequently the Raf kinase phosphorylates MEK kinase, and then, MEK phosphorylates and activates ERK.[66] The activated ERK phosphorylates various substrates and regulates various physiological functions of cells such as proliferation, differentiation, and survival.[67] Continuous extracellular stimulation may lead to the sustained activation of the MAPK pathway in the process of chronic inflammation.[68] In UC, the production of IL-2 and IFN-γ during inflammation can be alleviated by inhibiting the MAPK signaling pathway.[69,70] Our study found that AIL had no effect on Ras, MEK, p-MEK, and ERK1/2 but significantly reduced RAF-1, p-RAF-1, and p-ERK1/2 in activated Jurkat T cells. This suggested that RAF-1 may directly affect ERK1/2 to function and does not regulate MEK1/2, which is also supported by the literature.[71] The signal transducer and activator transcription 3 (STAT3) acts as an important downstream factor of the ERK1/2, which plays a complex regulatory role in inflammation and immune processes.[72] Under inflammatory stimulation, STAT3 is activated and translocated into the nucleus, where it binds to the promoter regions of inflammation-related genes to promote the expression of cytokines.[73,74] AIL suppressed phosphorylation of STAT3 to inhibit transcription of inflammatory factors in activated Jurkat T cells. In the early stages of the inflammatory response, the transcription factor activator protein-1 (AP-1) is activated by ERK to promote the transcription of inflammatory mediators such as IL-6, IL-2, and other genes and then to initiate the inflammatory response.[75] AP-1 consists of a diverse group of members including Jun, Fos, Maf, and ATF. The Jun family has three members, JunB, c-Jun, and JunD, in which c-Jun can be activated by ERK.[76] Our results showed that P/I did not increase c-JUN, although it significantly enhanced the phosphorylation of ERK and elevated inflammatory factors. Moreover, AIL dramatically reduced c-JUN in unactivated Jurkat T cells, while the inflammatory factors showed no change. Therefore, the expression of c-JUN may not affect the expression of inflammatory factors in this study. In general, in activated Jurkat T cells, we found that AIL could suppress the expression of IL-2 and IFN-γ by inhibiting the RAF/ERK/STAT3 signaling pathway.

The PI3K-AKT-mTOR pathway can regulate the production of inflammatory mediators such as cytokines and chemokines.[77] In UC, the overactivated PI3K-AKT pathway causes T cells to secrete excessive pro-inflammatory cytokines, such as IFN-γ and IL-17, which further exacerbate intestinal inflammation.[78] Nuclear factor κB (NF-κB) is a key transcription factor in the inflammatory response, which regulates the expression of various inflammation-related genes, including TNF-α, IFN-γ, IL-2, and other cytokines.[79,80] However, in this study, AIL had no impact on the PI3K-AKT-mTOR signaling pathway and the level of NF-κB, either in activated or unactivated Jurkat T cells. Although experimental results showed that AIL does not exert its anti-inflammatory and immunoregulatory effects by modulating the PI3K-AKT-mTOR signaling pathway or the expression of c-JUN and NF-κB, it cannot be excluded that other active components of JLW may regulate these targets to treat UC.

AIL exhibits excellent antiviral, anti-inflammation, antibacterial, and antitumor activities.[36] It has been reported that AIL could target *P*23 for the treatment of prostate cancer to overcome MDV3100-resistance in prostate cancer cell lines and has good drug-like properties, such as good bioavailability, high solubility, minimal CYP450 inhibition, and low hepatotoxicity at therapeutic doses.[81] However, in the acute toxicity experiment in mice, the LD_{50} for AIL was 27.2 mg/kg, and severe pathological damage was observed mainly in liver and gastrointestinal tract. Moreover, in a 28-day subacute toxicity study, a single dose of 10.0 mg/kg caused transient hepatic enzyme elevation, while repeated doses of 2.5 mg/kg administered every 48 h induced cumulative gastrointestinal toxicity.[82] These findings highlight the necessity of dose optimization to enhance the therapeutic safety of AIL.

5. CONCLUSIONS

In summary, this study predicted and validated the prominent components, core targets, and signal pathways of JLW in the treatment of UC through network pharmacology, molecular docking, and *in vitro* experiments. Network pharmacology and molecular docking results suggested that the prominent components of JLW may target AKT1, P53, STAT3, c-JUN, and ERK1 and treat UC through PI3K-AKT, MAPK, Ras, Rap1, TNF, T cell receptor, HIF-1, C-type lectin receptor, VEGF, and Th17 cell differentiation signal pathways. The *in vitro* experiments verified that the representative component AIL of JLW may inhibit the RAF/ERK/STAT3 signaling pathway and increase the phosphorylation of p53 to reduce the inflammation and excessive immunity of UC.

AUTHOR INFORMATION

Corresponding Authors

Mingzhi Zou − *The Key Laboratory of Sepsis Translational Medicine and Interdisciplinary Science Research Center of Western Guangdong, The Second Affiliated Hospital of Guangdong Medical University, Zhanjiang, Guangdong Province 524003, P.R. of China*; Phone: +86-0769-89190075; Email: zmzgdmu@163.com; Fax: +86-0769-89190075

Hongbo Liao − *Guangdong Provincial Key Laboratory of Research and Development of Natural Drugs, School of Pharmacy, Guangdong Medical University, Zhanjiang, Guangdong Province 524023, P.R. of China*; Email: liaohongbo2024@163.com

Xin Wu − *Dongguan Key Laboratory of Characteristic Research and Achievement Transformation of Integrated Chinese and Western Medicine for Prevention and Treatment to Common Diseases, The First Dongguan Affiliated Hospital of Guangdong Medical University, Guangdong Medical University, Dongguan, Guangdong Province 523000, P. R. of*

https://doi.org/10.1021/acsomega.5c00261
ACS Omega 2025, 10, 19598−19613

China; The Key Laboratory of Sepsis Translational Medicine, The Second Affiliated Hospital of Guangdong Medical University, Zhanjiang, Guangdong Province 524003, P.R. of China; orcid.org/0000-0002-7911-8508; Email: woodbirdlhb@163.com

Authors

Zhifang Liao − *Dongguan Key Laboratory of Characteristic Research and Achievement Transformation of Integrated Chinese and Western Medicine for Prevention and Treatment to Common Diseases, The First Dongguan Affiliated Hospital of Guangdong Medical University, Guangdong Medical University, Dongguan, Guangdong Province 523000, P. R. of China*

Xiao Liu − *Dongguan Key Laboratory of Characteristic Research and Achievement Transformation of Integrated Chinese and Western Medicine for Prevention and Treatment to Common Diseases, The First Dongguan Affiliated Hospital of Guangdong Medical University, Guangdong Medical University, Dongguan, Guangdong Province 523000, P. R. of China*

Linxuan Li − *Dongguan Key Laboratory of Characteristic Research and Achievement Transformation of Integrated Chinese and Western Medicine for Prevention and Treatment to Common Diseases, The First Dongguan Affiliated Hospital of Guangdong Medical University, Guangdong Medical University, Dongguan, Guangdong Province 523000, P. R. of China; The Key Laboratory of Sepsis Translational Medicine and Interdisciplinary Science Research Center of Western Guangdong, The Second Affiliated Hospital of Guangdong Medical University, Zhanjiang, Guangdong Province 524003, P.R. of China*

Sikai Li − *Dongguan Key Laboratory of Characteristic Research and Achievement Transformation of Integrated Chinese and Western Medicine for Prevention and Treatment to Common Diseases, The First Dongguan Affiliated Hospital of Guangdong Medical University, Guangdong Medical University, Dongguan, Guangdong Province 523000, P. R. of China*

Xingxing Xing − *Dongguan Key Laboratory of Characteristic Research and Achievement Transformation of Integrated Chinese and Western Medicine for Prevention and Treatment to Common Diseases, The First Dongguan Affiliated Hospital of Guangdong Medical University, Guangdong Medical University, Dongguan, Guangdong Province 523000, P. R. of China*

Xiwen Zheng − *Dongguan Key Laboratory of Characteristic Research and Achievement Transformation of Integrated Chinese and Western Medicine for Prevention and Treatment to Common Diseases, The First Dongguan Affiliated Hospital of Guangdong Medical University, Guangdong Medical University, Dongguan, Guangdong Province 523000, P. R. of China*

Wenyu Song − *Dongguan Key Laboratory of Characteristic Research and Achievement Transformation of Integrated Chinese and Western Medicine for Prevention and Treatment to Common Diseases, The First Dongguan Affiliated Hospital of Guangdong Medical University, Guangdong Medical University, Dongguan, Guangdong Province 523000, P. R. of China*

Pin Gui − *Dongguan Key Laboratory of Characteristic Research and Achievement Transformation of Integrated Chinese and Western Medicine for Prevention and Treatment to Common Diseases, The First Dongguan Affiliated Hospital of Guangdong Medical University, Guangdong Medical University, Dongguan, Guangdong Province 523000, P. R. of China*

Qi Liu − *Dongguan Key Laboratory of Characteristic Research and Achievement Transformation of Integrated Chinese and Western Medicine for Prevention and Treatment to Common Diseases, The First Dongguan Affiliated Hospital of Guangdong Medical University, Guangdong Medical University, Dongguan, Guangdong Province 523000, P. R. of China*

Guanghong Rong − *Dongguan Key Laboratory of Characteristic Research and Achievement Transformation of Integrated Chinese and Western Medicine for Prevention and Treatment to Common Diseases, The First Dongguan Affiliated Hospital of Guangdong Medical University, Guangdong Medical University, Dongguan, Guangdong Province 523000, P. R. of China*

Yiming Shao − *Dongguan Key Laboratory of Characteristic Research and Achievement Transformation of Integrated Chinese and Western Medicine for Prevention and Treatment to Common Diseases, The First Dongguan Affiliated Hospital of Guangdong Medical University, Guangdong Medical University, Dongguan, Guangdong Province 523000, P. R. of China; The Key Laboratory of Sepsis Translational Medicine, The Second Affiliated Hospital of Guangdong Medical University, Zhanjiang, Guangdong Province 524003, P.R. of China*

Complete contact information is available at: https://pubs.acs.org/10.1021/acsomega.5c00261

Author Contributions

[1]Z.L. and X.L. contributed equally to this work and share first authorship.

Author Contributions

Z.L. and X.L. contributed equally to this work and were co-first authors. X.W., H.L., and M.Z. proposed the ideas and designed the experiments. Z.L., X.L., L.L., X.Z., and W.S. analyzed the data. P.G., Q.L., G.R., and Y.S. supervised the study. Z.L., X.L., L.L., S.L., and X.X. conducted the experiments. X.W., M.Z., and Y.S. acquired the funding. Z.L. and X.L. wrote the original draft preparation. X.W. and H.L. reviewed and edited the manuscript.

Notes

The authors declare no competing financial interest.

■ ACKNOWLEDGMENTS

This work was supported by the Key Research Laboratory and Key Discipline Development Project for Traditional Chinese Medicine in the Prevention and Treatment of Infectious Diseases of Traditional Chinese Medicine Bureau of Guangdong Province (Grant no. 2023337), the Science and Technology Planning Project of Zhangjiang Municipality (Grant no. 2021A05092, 2021A05097, and 2022A01148), the Discipline Construction Project of Guangdong Medical University (Grant no. GDMXK2021002, GDMXK2021003), the Science and Technology Planning Project of Shenzhen Municipality (Grant no. JCYJ20190806154207168), and the Talent Development Foundation of The First Dongguan Affiliated Hospital of Guangdong Medical University (Grant no. GCC2023022).

REFERENCES

(1) Le Berre, C.; Honap, S.; Peyrin-Biroulet, L. Ulcerative colitis. *Lancet* **2023**, *402* (10401), 571−584.
(2) Ordas, I.; Eckmann, L.; Talamini, M.; Baumgart, D. C.; Sandborn, W. J. Ulcerative colitis. *Lancet* **2012**, *380* (9853), 1606−1619.
(3) Ungaro, R.; Mehandru, S.; Allen, P. B.; Peyrin-Biroulet, L.; Colombel, J. F. Ulcerative colitis. *Lancet* **2017**, *389* (10080), 1756−1770.
(4) Del Sordo, R.; Lougaris, V.; Bassotti, G.; Armuzzi, A.; Villanacci, V. Therapeutic agents affecting the immune system and drug-induced inflammatory bowel disease (IBD): A review on etiological and pathogenetic aspects. *Clin Immunol* **2022**, *234*, No. 108916.
(5) de Lange, K. M.; Moutsianas, L.; Lee, J. C.; Lamb, C. A.; Luo, Y.; Kennedy, N. A.; Jostins, L.; Rice, D. L.; Gutierrez-Achury, J.; Ji, S. G.; et al. Genome-wide association study implicates immune activation of multiple integrin genes in inflammatory bowel disease. *Nat. Genet.* **2017**, *49* (2), 256−261.
(6) Fachal, L.; International IBD Genetics Consortium. OPP11 Expanded genome-wide association study of Inflammatory Bowel Disease identifies 174 novel loci and directly implicates new genes in disease susceptibility. *J. Crohn's Colitis* **2022**, *16* (Supplement_1), i011−i013.
(7) Sazonovs, A.; Stevens, C. R.; Venkataraman, G. R.; Yuan, K.; Avila, B.; Abreu, M. T.; Ahmad, T.; Allez, M.; Ananthakrishnan, A. N.; Atzmon, G.; et al. Large-scale sequencing identifies multiple genes and rare variants associated with Crohn's disease susceptibility. *Nat. Genet.* **2022**, *54* (9), 1275−1283.
(8) Berends, S. E.; Strik, A. S.; Löwenberg, M.; D'Haens, G. R.; Mathôt, R. A. A. Clinical Pharmacokinetic and Pharmacodynamic Considerations in the Treatment of Ulcerative Colitis. *Clin Pharmacokinet* **2019**, *58* (1), 15−37.
(9) Kobayashi, T.; Siegmund, B.; Le Berre, C.; Wei, S. C.; Ferrante, M.; Shen, B.; Bernstein, C. N.; Danese, S.; Peyrin-Biroulet, L.; Hibi, T. Ulcerative colitis. *Nat. Rev. Dis. Primers* **2020**, *6* (1), 74.
(10) Burri, E.; Maillard, M. H.; Schoepfer, A. M.; Seibold, F.; Van Assche, G.; Rivière, P.; Laharie, D.; Manz, M. Treatment Algorithm for Mild and Moderate-to-Severe Ulcerative Colitis: An Update. *Digestion* **2020**, *101* (Suppl 1), 2−15.
(11) Bhattacharya, A.; Osterman, M. T. Biologic Therapy for Ulcerative Colitis. *Gastroenterol Clin North Am.* **2020**, *49* (4), 717−729.
(12) Liu, Y.; Li, B. G.; Su, Y. H.; Zhao, R. X.; Song, P.; Li, H.; Cui, X. H.; Gao, H. M.; Zhai, R. X.; Fu, X. J.; et al. Potential activity of Traditional Chinese Medicine against Ulcerative colitis: A review. *J. Ethnopharmacol* **2022**, *289*, No. 115084.
(13) Zhang, S.; Zhao, L.; Shen, H.; Tang, Z.; Qin, D.; Li, J.; Zhang, B.; Yang, G.; Chen, M.; Wu, K.; et al. International clinical practice guideline on the use of traditional Chinese medicine for ulcerative colitis by Board of Specialty Committee of Digestive System Disease of World Federation of Chinese Medicine Societies (2023). *Phytother Res.* **2024**, *38* (2), 970−999.
(14) Li, M.-Y.; Luo, H.-J.; Wu, X.; Liu, Y.-H.; Gan, Y.-X.; Xu, N.; Zhang, Y.-M.; Zhang, S.-H.; Zhou, C.-L.; Su, Z.-R.; et al. Anti-Inflammatory Effects of Huangqin Decoction on Dextran Sulfate Sodium-Induced Ulcerative Colitis in Mice Through Regulation of the Gut Microbiota and Suppression of the Ras-PI3K-Akt-HIF-1alpha and NF-kappaB Pathways. *Front. Pharmacol.* **2019**, *10*, 1552.
(15) Luo, S.; Wen, R.; Wang, Q.; Zhao, Z.; Nong, F.; Fu, Y.; Huang, S.; Chen, J.; Zhou, L.; Luo, X. Rhubarb Peony Decoction ameliorates ulcerative colitis in mice by regulating gut microbiota to restoring Th17/Treg balance. *J. Ethnopharmacol* **2019**, *231*, 39−49.
(16) Shen, Y.; Zou, J.; Chen, M.; Zhang, Z.; Liu, C.; Jiang, S.; Qian, D.; Duan, J. A. Protective effects of Lizhong decoction on ulcerative colitis in mice by suppressing inflammation and ameliorating gut barrier. *J. Ethnopharmacol* **2020**, *259*, No. 112919.
(17) Dai, Y.; Lu, Q.; Li, P.; Zhu, J.; Jiang, J.; Zhao, T.; Hu, Y.; Ding, K.; Zhao, M. Xianglian Pill attenuates ulcerative colitis through TLR4/MyD88/NF-kappaB signaling pathway. *J. Ethnopharmacol* **2023**, *300*, No. 115690.
(18) Chen, M.; Ding, Y.; Tong, Z. Efficacy and Safety of Sophora flavescens (Kushen) Based Traditional Chinese Medicine in the Treatment of Ulcerative Colitis: Clinical Evidence and Potential Mechanisms. *Front Pharmacol* **2020**, *11*, No. 603476.
(19) Peng, K. Y.; Gu, J. F.; Su, S. L.; Zhu, Y.; Guo, J. M.; Qian, D. W.; Duan, J. A. Salvia miltiorrhiza stems and leaves total phenolic acids combination with tanshinone protect against DSS-induced ulcerative colitis through inhibiting TLR4/PI3K/AKT/mTOR signaling pathway in mice. *J. Ethnopharmacol* **2021**, *264*, No. 113052.
(20) Cheng, H.; Zhang, D.; Wu, J.; Liu, J.; Tan, Y.; Feng, W.; Peng, C. Atractylodes macrocephala Koidz. volatile oil relieves acute ulcerative colitis via regulating gut microbiota and gut microbiota metabolism. *Front. Immunol.* **2023**, *14*, No. 1127785.
(21) Chao, L.; Lin, J.; Zhou, J.; Du, H.; Chen, X.; Liu, M.; Qu, Q.; Lv, W.; Guo, S. Polyphenol Rich Forsythia suspensa Extract Alleviates DSS-Induced Ulcerative Colitis in Mice through the Nrf2-NLRP3 Pathway. *Antioxidants* **2022**, *11* (3), 475.
(22) Huang, Y. F.; Zhou, J. T.; Qu, C.; Dou, Y. X.; Huang, Q. H.; Lin, Z. X.; Xian, Y. F.; Xie, J. H.; Xie, Y. L.; Lai, X. P.; et al. Anti-inflammatory effects of Brucea javanica oil emulsion by suppressing NF-kappaB activation on dextran sulfate sodium-induced ulcerative colitis in mice. *J. Ethnopharmacol* **2017**, *198*, 389−398.
(23) Li, Y. Y.; Wang, X. J.; Su, Y. L.; Wang, Q.; Huang, S. W.; Pan, Z. F.; Chen, Y. P.; Liang, J. J.; Zhang, M. L.; Xie, X. Q.; et al. Baicalein ameliorates ulcerative colitis by improving intestinal epithelial barrier via AhR/IL-22 pathway in ILC3s. *Acta Pharmacol Sin* **2022**, *43* (6), 1495−1507.
(24) Li, B.; Du, P.; Du, Y.; Zhao, D.; Cai, Y.; Yang, Q.; Guo, Z. Luteolin alleviates inflammation and modulates gut microbiota in ulcerative colitis rats. *Life Sci.* **2021**, *269*, No. 119008.
(25) Yang, Y.; Zhang, Y.; Song, J.; Li, Y.; Zhou, L.; Xu, H.; Wu, K.; Gao, J.; Zhao, M.; Zheng, Y. Bergamot polysaccharides relieve DSS-induced ulcerative colitis via regulating the gut microbiota and metabolites. *Int. J. Biol. Macromol.* **2023**, *253* (Pt 7), No. 127335.
(26) Wan, L.; Qian, C.; Yang, C.; Peng, S.; Dong, G.; Cheng, P.; Zong, G.; Han, H.; Shao, M.; Gong, G.; et al. Ginseng polysaccharides ameliorate ulcerative colitis via regulating gut microbiota and tryptophan metabolism. *Int. J. Biol. Macromol.* **2024**, *265* (Pt 2), No. 130822.
(27) Yang, N.; Xia, Z.; Shao, N.; Li, B.; Xue, L.; Peng, Y.; Zhi, F.; Yang, Y. Carnosic acid prevents dextran sulfate sodium-induced acute colitis associated with the regulation of the Keap1/Nrf2 pathway. *Sci. Rep.* **2017**, *7* (1), 11036.
(28) Zhou, Z.; He, W.; Tian, H.; Zhan, P.; Liu, J. Thyme (Thymus vulgaris L.) polyphenols ameliorate DSS-induced ulcerative colitis of mice by mitigating intestinal barrier damage, regulating gut microbiota, and suppressing TLR4/NF-kappaB-NLRP3 inflammasome pathways. *Food Funct* **2023**, *14* (2), 1113−1132.
(29) Ran, X. F. *National Formulary of Proprietary Chinese Medicines*; National Formulary of Proprietary Chinese Medicines, **1962**.
(30) Zhang, S.; Li, G. Progress of research on the pathogenesis of prolonged dysentery in traditional Chinese medicine in the past 5 years. *Inn. Mong. Tradit. Chin. Med.* **2016**, *35* (7), 142.
(31) Noor, F.; Asif, M.; Ashfaq, U. A.; Qasim, M.; Ul Qamar, M. T. Machine learning for synergistic network pharmacology: a comprehensive overview. *Brief Bioinf.* **2023**, *24* (3), No. bbad120.
(32) Zhao, L.; Zhang, H.; Li, N.; Chen, J.; Xu, H.; Wang, Y.; Liang, Q. Network pharmacology, a promising approach to reveal the pharmacology mechanism of Chinese medicine formula. *J. Ethnopharmacol* **2023**, *309*, No. 116306.
(33) Ravindranath, P. A.; Forli, S.; Goodsell, D. S.; Olson, A. J.; Sanner, M. F. AutoDockFR: Advances in Protein-Ligand Docking with Explicitly Specified Binding Site Flexibility. *PLoS Comput. Biol.* **2015**, *11* (12), No. e1004586.
(34) Mohd Jamil, M. D. H.; Taher, M.; Susanti, D.; Rahman, M. A.; Zakaria, Z. A. Phytochemistry, Traditional Use and Pharmacological

https://doi.org/10.1021/acsomega.5c00261
ACS Omega 2025, 10, 19598−19613

Activity of Picrasma quassioides: A Critical Reviews. *Nutrients* **2020**, *12* (9), 2584.
(35) Xu, W. H.; Liang, Z. S.; Su, X. M.; He, R. X.; Liang, Q. Genus Picrasma: A comprehensive review on its ethnopharmacology, phytochemistry and bioactivities. *J. Ethnopharmacol* **2021**, *280*, No. 114441.
(36) Li, X.; Li, Y.; Ma, S.; Zhao, Q.; Wu, J.; Duan, L.; Xie, Y.; Wang, S. Traditional uses, phytochemistry, and pharmacology of Ailanthus altissima (Mill.) Swingle bark: A comprehensive review. *J. Ethnopharmacol* **2021**, *275*, No. 114121.
(37) Moorton, M.; Tng, P. Y. L.; Inoue, R.; Netherton, C. L.; Gerner, W.; Schmidt, S. Investigation of activation-induced markers (AIM) in porcine T cells by flow cytometry. *Front. Vet. Sci.* **2024**, *11*, No. 1390486.
(38) Kuca-Warnawin, E.; Janicka, I.; Szczęsny, P.; Olesińska, M.; Bonek, K.; Głuszko, P.; Kontny, E. Modulation of T-Cell Activation Markers Expression by the Adipose Tissue−Derived Mesenchymal Stem Cells of Patients with Rheumatic Diseases. *Cell Transplant.* **2020**, *29*, 963689720945682.
(39) Chaudhry, S.; Freebern, W. J.; Smith, J. L.; Butscher, W. G.; Haggerty, C. M.; Gardner, K. Cross-regulation of T cell growth factor expression by p53 and the Tax oncogene. *J. Immunol* **2002**, *169* (12), 6767−6778.
(40) Fischer, M.; Sammons, M. A. Determinants of p53 DNA binding, gene regulation, and cell fate decisions. *Cell Death Differ.* **2024**, *31* (7), 836−843.
(41) Gros, B.; Kaplan, G. G. Ulcerative Colitis in Adults: A Review. *JAMA* **2023**, *330* (10), 951−965.
(42) Ramos, G. P.; Papadakis, K. A. Mechanisms of Disease: Inflammatory Bowel Diseases. *Mayo Clin Proc.* **2019**, *94* (1), 155−165.
(43) Bouma, G.; Strober, W. The immunological and genetic basis of inflammatory bowel disease. *Nat. Rev. Immunol* **2003**, *3* (7), 521−533.
(44) Wang, M.; Fu, R.; Xu, D.; Chen, Y.; Yue, S.; Zhang, S.; Tang, Y. Traditional Chinese Medicine: A promising strategy to regulate the imbalance of bacterial flora, impaired intestinal barrier and immune function attributed to ulcerative colitis through intestinal microecology. *J. Ethnopharmacol.* **2024**, *318* (Pt A), No. 116879.
(45) Wang, T.; Liu, X.; Zhang, W.; Wang, J.; Wang, T.; Yue, W.; Ming, L.; Cheng, J.; Sun, J. Traditional Chinese medicine treats ulcerative colitis by regulating gut microbiota, signaling pathway and cytokine: Future novel method option for pharmacotherapy. *Heliyon* **2024**, *10* (6), No. e27530.
(46) Zhang, C.; Jiang, M.; Lu, A. Considerations of traditional Chinese medicine as adjunct therapy in the management of ulcerative colitis. *Clin Rev. Allergy Immunol* **2013**, *44* (3), 274−283.
(47) Li, S.; Zhang, B. Traditional Chinese medicine network pharmacology: theory, methodology and application. *Chin J. Nat. Med.* **2013**, *11* (2), 110−120.
(48) Li, C. Y.; Chao, L. K.; Wang, S. C.; Chang, H. Z.; Tsai, M. L.; Fang, S. H.; Liao, P. C.; Ho, C. L.; Chen, S. T.; Cheng, W. C.; et al. Honokiol inhibits LPS-induced maturation and inflammatory response of human monocyte-derived dendritic cells. *J. Cell Physiol* **2011**, *226* (9), 2338−2349.
(49) Li, L.; Xu, S.; Wang, W.; Li, X.; Wang, H.; Yang, Q.; Wang, C.; Gu, J.; Luo, H.; Meng, Q. Bruceine A alleviates alcoholic liver disease by inhibiting AIM2 inflammasome activation via activating FXR. *Phytomedicine* **2024**, *130*, No. 155693.
(50) Liu, Z.; Guo, L.; Zhu, X.; Li, X.; Zhao, W.; Yu, P.; Teng, Y. Palmatine ameliorates cisplatin-induced acute kidney injury through regulating Akt and NF-κB/MAPK pathways. *Arabian J. Chem.* **2024**, *17* (5), No. 105731.
(51) Ma, S. B.; Liu, L.; Li, X.; Xie, Y. H.; Shi, X. P.; Wang, S. W. Virtual screening-molecular docking-activity evaluation of Ailanthus altissima (Mill.) swingle bark in the treatment of ulcerative colitis. *BMC Complementary Med. Ther.* **2023**, *23* (1), 197.
(52) Nam, K. N.; Kim, K. P.; Cho, K. H.; Jung, W. S.; Park, J. M.; Cho, S. Y.; Park, S. K.; Park, T. H.; Kim, Y. S.; Lee, E. H. Prevention of inflammation-mediated neurotoxicity by butylidenephthalide and its role in microglial activation. *Cell Biochem Funct* **2013**, *31* (8), 707−712.
(53) Park, E. J.; Park, S. W.; Kim, H. J.; Kwak, J. H.; Lee, D. U.; Chang, K. C. Dehydrocostuslactone inhibits LPS-induced inflammation by p38MAPK-dependent induction of hemeoxygenase-1 in vitro and improves survival of mice in CLP-induced sepsis in vivo. *Int. Immunopharmacol* **2014**, *22* (2), 332−340.
(54) Richard, S. A. Exploring the Pivotal Immunomodulatory and Anti-Inflammatory Potentials of Glycyrrhizic and Glycyrrhetinic Acids. *Mediators Inflammation* **2021**, *2021*, No. 6699560.
(55) Shi, Y.; Chen, J.; Li, S.; Wu, Y.; Yu, C.; Ni, L.; Xiao, J.; Shao, Z.; Zhu, H.; Wang, J.; et al. Tangeretin suppresses osteoarthritis progression via the Nrf2/NF-kappaB and MAPK/NF-kappaB signaling pathways. *Phytomedicine* **2022**, *98*, No. 153928.
(56) Yuan, C.; Yu, C.; Sun, Q.; Xiong, M.; Ren, B.; Zhong, M.; Peng, Q.; Zeng, M.; Meng, P.; Li, L.; et al. Atractylenolide I Alleviates Indomethacin-Induced Gastric Ulcers in Rats by Inhibiting NLRP3 Inflammasome Activation. *J. Agric. Food Chem.* **2024**, *72* (25), 14165−14176.
(57) Zhang, Y.; Wang, X.; Yang, X.; Yang, X.; Xue, J.; Yang, Y. Ganoderic Acid A To Alleviate Neuroinflammation of Alzheimer's Disease in Mice by Regulating the Imbalance of the Th17/Tregs Axis. *J. Agric. Food Chem.* **2021**, *69* (47), 14204−14214.
(58) Oh, H. M.; Lee, S. W.; Park, M. H.; Kim, M. H.; Ryu, Y. B.; Kim, M. S.; Kim, H. H.; Park, K. H.; Lee, W. S.; Park, S. J.; et al. Norkurarinol inhibits toll-like receptor 3 (TLR3)-mediated pro-inflammatory signaling pathway and rotavirus replication. *J. Pharmacol Sci.* **2012**, *118* (2), 161−170.
(59) Smith-Garvin, J. E.; Koretzky, G. A.; Jordan, M. S. T cell activation. *Annu. Rev. Immunol.* **2009**, *27*, 591−619.
(60) Gao, R.; Li, X.; Gao, H.; Zhao, K.; Liu, X.; Liu, J.; Wang, Q.; Zhu, Y.; Chen, H.; Xiang, S.; et al. Protein phosphatase 2A catalytic subunit beta suppresses PMA/ionomycin-induced T-cell activation by negatively regulating PI3K/Akt signaling. *FEBS J.* **2022**, *289* (15), 4518−4535.
(61) Wieland, E.; Shipkova, M. Lymphocyte surface molecules as immune activation biomarkers. *Clin Biochem* **2016**, *49* (4−5), 347−354.
(62) Stritesky, G. L.; Jameson, S. C.; Hogquist, K. A. Selection of self-reactive T cells in the thymus. *Annu. Rev. Immunol.* **2012**, *30*, 95−114.
(63) Mimitou, E. P.; Lareau, C. A.; Chen, K. Y.; Zorzetto-Fernandes, A. L.; Hao, Y.; Takeshima, Y.; Luo, W.; Huang, T. S.; Yeung, B. Z.; Papalexi, E.; et al. Scalable, multimodal profiling of chromatin accessibility, gene expression and protein levels in single cells. *Nat. Biotechnol.* **2021**, *39* (10), 1246−1258.
(64) Katsuyama, T.; Tsokos, G. C.; Moulton, V. R. Aberrant T Cell Signaling and Subsets in Systemic Lupus Erythematosus. *Front. Immunol.* **2018**, *9*, 1088.
(65) Cope, A. P. Exploring the reciprocal relationship between immunity and inflammation in chronic inflammatory arthritis. *Rheumatology (Oxford)* **2003**, *42* (6), 716−731.
(66) Junttila, M. R.; Li, S. P.; Westermarck, J. Phosphatase-mediated crosstalk between MAPK signaling pathways in the regulation of cell survival. *FASEB J.* **2008**, *22* (4), 954−965.
(67) Cargnello, M.; Roux, P. P. Activation and function of the MAPKs and their substrates, the MAPK-activated protein kinases. *Microbiol Mol. Biol. Rev.* **2011**, *75* (1), 50−83.
(68) Yu, L.; Yan, J.; Sun, Z. D-limonene exhibits anti-inflammatory and antioxidant properties in an ulcerative colitis rat model via regulation of iNOS, COX-2, PGE2 and ERK signaling pathways. *Mol. Med. Rep* **2017**, *15* (4), 2339−2346.
(69) Yuan, Y.; Wu, H.; Shuai, B.; Liu, C.; Zhu, F.; Gao, F.; Wei, C.; Fan, H. Mechanism of HSP90 Inhibitor in the Treatment of DSS-induced Colitis in Mice by Inhibiting MAPK Pathway and Synergistic Effect of Compound Sophorae Decoction. *Curr. Pharm. Des* **2022**, *28* (42), 3456−3468.
(70) Wang, Y.; Qin, J.; Dong, L.; He, C.; Zhang, D.; Wu, X.; Li, T.; Yue, H.; Mu, L.; Wang, Q.; et al. Suppression of mir-150−5p

https://doi.org/10.1021/acsomega.5c00261
ACS Omega 2025, 10, 19598−19613

attenuates the anti-inflammatory effect of glucocorticoids in mice with ulcerative colitis. *Mol. Immunol* **2023**, *163*, 28−38.
(71) Luo, Q.; Gu, Y.; Zheng, W.; Wu, X.; Gong, F.; Gu, L.; Sun, Y.; Xu, Q. Erlotinib inhibits T-cell-mediated immune response via down-regulation of the c-Raf/ERK cascade and Akt signaling pathway. *Toxicol. Appl. Pharmacol.* **2011**, *251* (2), 130−136.
(72) Kuroki, M.; O'Flaherty, J. T. Extracellular signal-regulated protein kinase (ERK)-dependent and ERK-independent pathways target STAT3 on serine-727 in human neutrophils stimulated by chemotactic factors and cytokines. *Biochem. J.* **1999**, *341* (Pt3), 691−696.
(73) Kaminska, B.; Mota, M.; Pizzi, M. Signal transduction and epigenetic mechanisms in the control of microglia activation during neuroinflammation. *Biochim. Biophys. Acta* **2016**, *1862* (3), 339−351.
(74) Pan, J.; Zhou, L.; Zhang, C.; Xu, Q.; Sun, Y. Targeting protein phosphatases for the treatment of inflammation-related diseases: From signaling to therapy. *Signal Transduction Targeted Ther.* **2022**, *7* (1), 177.
(75) Kida, Y.; Kobayashi, M.; Suzuki, T.; Takeshita, A.; Okamatsu, Y.; Hanazawa, S.; Yasui, T.; Hasegawa, K. Interleukin-1 stimulates cytokines, prostaglandin E2 and matrix metalloproteinase-1 production via activation of MAPK/AP-1 and NF-kappaB in human gingival fibroblasts. *Cytokine* **2005**, *29* (4), 159−168.
(76) Song, D.; Lian, Y.; Zhang, L. The potential of activator protein 1 (AP-1) in cancer targeted therapy. *Front. Immunol.* **2023**, *14*, No. 1224892.
(77) Yu, J. S.; Cui, W. Proliferation, survival and metabolism: the role of PI3K/AKT/mTOR signalling in pluripotency and cell fate determination. *Development* **2016**, *143* (17), 3050−3060.
(78) Ni, L.; Lu, Q.; Tang, M.; Tao, L.; Zhao, H.; Zhang, C.; Yu, Y.; Wu, X.; Liu, H.; Cui, R. Periplaneta americana extract ameliorates dextran sulfate sodium-induced ulcerative colitis via immunoregulatory and PI3K/AKT/NF-kappaB signaling pathways. *Inflammopharmacology* **2022**, *30* (3), 907−918.
(79) Barnabei, L.; Laplantine, E.; Mbongo, W.; Rieux-Laucat, F.; Weil, R. NF-kappaB: At the Borders of Autoimmunity and Inflammation. *Front Immunol* **2021**, *12*, No. 716469.
(80) He, X.; Li, Y.; Deng, B.; Lin, A.; Zhang, G.; Ma, M.; Wang, Y.; Yang, Y.; Kang, X. The PI3K/AKT signalling pathway in inflammation, cell death and glial scar formation after traumatic spinal cord injury: Mechanisms and therapeutic opportunities. *Cell Proliferation* **2022**, *55* (9), No. e13275.
(81) He, Y.; Peng, S.; Wang, J.; Chen, H.; Cong, X.; Chen, A.; Hu, M.; Qin, M.; Wu, H.; Gao, S.; et al. Ailanthone targets p23 to overcome MDV3100 resistance in castration-resistant prostate cancer. *Nat. Commun.* **2016**, *7*, 13122.
(82) Tang, S. Studies on the General Toxicityand Toxicokinetics of Ailanthone. M.D. Dissertation, East China Normal University: Pu tuo, Shang hai, 2018. https://kns.cnki.net/kcms2/article/abstract?v=tOz5m-jLbAVL7iKGcGNP8Htfv0lwXpYGbnoXAykctwZl2rVM2oZ11OjPEAh1Ht8mkDJl163PJicK_UzN8Q_9v5-TOtKphaYfTpxo9iewbEcgTwnRJQeWF4u09cHaEgG6KPK-V10Yw1r64TD9dxvppQqv3v8oLM_p9Wnh-kZsT2HkxGoI0kVWEYYAxLix6IOdReJn_F_NYEkM=&uniplatform=NZKPT&language=CHS.

https://doi.org/10.1021/acsomega.5c00261
ACS Omega 2025, 10, 19598−19613